

NUCLEATION AND CRYSTAL GROWTH OF  
CALCIUM SULFITE HEMIHYDRATE

BY

Cynthia Lynn Gleason, B.S., M.S.

DISSERTATION

Presented to the Faculty of the Graduate School of  
The University of Texas at Austin  
in Partial Fulfillment  
of the Requirements  
for the Degree of

DOCTOR OF PHILOSOPHY

THE UNIVERSITY OF TEXAS AT AUSTIN  
August 1989

## ACKNOWLEDGEMENTS

I wish to thank Dr. Gary T. Rochelle for his patience, understanding and guidance over the past several years. Many thanks go to all the friends I've made here - some of which have left before me: Cini Gage, Jim Critchfield, Joe Peterson, Woytek Jozewicz, Charlotte Stromblad, David Austgen, David Glasscock, David Tremple, Will White, Jerry Toman, Stephen Beaudoin, Paul Chu, Rob Shiely, Brett Hanson, Rosa Ruiz-Alsop, Philip Tseng and Yungli Lee. Ya'll have made graduate school worth while.

This research would not have been possible without the moral and financial support of my husband, Bill Gleason. I truly appreciate the sacrifices he's made so I could continue my education.

Thanks also go to the FGD various donors who supported this research and provided funds to attend the FGD Symposia.

particle size. This would lead to an improved sludge quality and lower disposal costs. The nucleation and crystal growth rates of calcium sulfite hemihydrate were measured in a continuous flow crystallizer. The effects of solution sulfate concentration, residence time, suspension density and temperature on the rates were investigated. It was determined that the nucleation rate was directly proportional to the suspension density. The particle size distribution does not change when the suspension density is changed. The growth rate was found to be directly proportional to the solids residence time in the reactor. Therefore, particle size distribution cannot be increased by increasing the residence time in the reactor.. The activation energy for  $\text{CaSO}_3 \frac{1}{2} \text{H}_2\text{O}$  nucleation was estimated to be 4 kcal/mole within the temperature range of 25 to 55 °C. The nucleation rate constant was pH dependent and had a maximum near pH 5.5. Sulfate in solution inhibited nucleation. It was observed that there was a maximum in the nucleation rate constant at pH 5.5.

## NUCLEATION AND CRYSTAL GROWTH OF CALCIUM SULFITE HEMIHYDRATE

Publication No. \_\_\_\_\_

Cynthia Lynn Gleason, Ph.D.  
The University of Texas at Austin, 1989

Supervising Professor: Gary T. Rochelle

The rates of calcium sulfite dissolution, nucleation and crystal growth are important in slurry scrubbing processes for flue gas desulfurization. The rates affect the scrubber solution composition, SO<sub>2</sub> absorption, sulfite oxidation, and limestone utilization. Sludge disposal is a significant cost in most slurry scrubbing processes for flue gas desulfurization. The settling rate and settled density of the sludge are related to the particle size distribution of the calcium sulfite particles.

The dissolution and precipitation rates of platelet shaped calcium sulfite crystals were measured in a pH stat apparatus. The solution pH was varied from 3.0 to 6.0. The effects of sulfate content in the solids and solution were also investigated. The measured rates for the platelets were compared to the rates previously determined for agglomerates. It was determined that there are subtle differences between platelet and agglomerated calcium sulfite. The platelet sample with a low solid sulfate content dissolved and crystallized slower than the platelet sample with a high solid sulfate content. Low sulfate platelets also dissolved and crystallized slower than the agglomerated samples. The inhibiting effect of dissolved sulfate was also greater for the sample with low solid sulfate. The sample with high solid sulfate dissolved and crystallized at approximately the same rate as the agglomerates.

Size distributions can be predicted if nucleation and growth rates are known. These rates can also be used to examine prospects for increasing the calcium sulfite

## Table of Contents

Acknowledgements . . . . .	v
Abstract . . . . .	vi
Table of Contents . . . . .	viii
List of Figures . . . . .	xi
List of Tables . . . . .	xii
Chapter 1. Background of Research . . . . .	1
1.1 Overview of Flue Gas Desulfurization . . . . .	1
1.1.1 Lime/Limestone Slurry Scrubbing . . . . .	1
1.1.2 Clear Solution Scrubbing . . . . .	3
1.1.3 Lime Spray Drying . . . . .	4
1.2 Previous work . . . . .	6
1.2.1 Dissolution and Precipitation . . . . .	6
1.2.2 Nucleation and Crystal Growth . . . . .	7
1.3 Scope of Investigation . . . . .	11
Chapter 2. Batch Experiments with Platelets . . . . .	12
2.1 Summary . . . . .	12
2.2 Dissolution . . . . .	12
2.2.1 Theory . . . . .	12
2.2.2 Seed Crystal Characterization . . . . .	14
2.2.3 Experimental Apparatus and Procedure . . . . .	15
2.2.4 Results and Discussion . . . . .	20

2.2.4.1	Effects of Particle Size, Shape and Sulfate Content in Solids . . . . .	20
2.2.4.2	Effect of Dissolved Sulfate . . . . .	24
2.3	Crystallization . . . . .	25
2.3.1	Experimental Apparatus and Procedure . . . . .	25
2.3.2	Results and Discussion . . . . .	26
2.3.2.1	Crystallization Rate Correlation . . . . .	26
2.3.2.2	Effect of Gypsum Saturation . . . . .	28
2.4	Nomenclature . . . . .	30
Chapter 3.	Nucleation and Crystal Growth . . . . .	31
3.1	Summary . . . . .	31
3.2	Theory . . . . .	32
3.2.1	Nucleation . . . . .	32
3.2.2	Crystal Growth . . . . .	33
3.2.3	Population Balance . . . . .	34
3.3	Experimental Apparatus and Procedure . . . . .	35
3.4	Results and Discussion . . . . .	39
3.4.1	Effect of Residence Time . . . . .	41
3.4.2	Effect of Suspension Density . . . . .	43
3.4.3	Effect of Temperature and pH . . . . .	46
3.4.4	Effect of Gypsum Saturation . . . . .	48
3.4.5	Growth Rate Correlation . . . . .	50
3.4.6	Three Feed System . . . . .	50
3.5	Nomenclature . . . . .	53
Chapter 4.	Conclusions and Recommendations . . . . .	54
4.1	Dissolution and Crystallization. . . . .	54
4.2	Nucleation and Crystal Growth . . . . .	54
4.3	Industrial Applications . . . . .	55
4.4	Recommendations for Future Work . . . . .	56

Appendix A. Analytical Methods	58
A.1 Iodimetric Titration	58
A.2 Coulter Counter Methods	59
Appendix B. Experimental Data	61
B.1 Dissolution Experiments	61
B.2 Crystallization Experiments	63
B.3 Nucleation and Crystal Growth Experiments	64
Appendix C. Error Analysis	68
B.1 Coulter Counter Measurements	68
B.2 Power law Equation	69
References	70

## List of Figures

Figure no.	Title	Page
1.1	Simple Slurry Scrubbing . . . . .	2
1.2	Dual Alkali Process . . . . .	4
1.3	Spray Drying Process . . . . .	5
2.1	SEM Photograph - Sample 1 . . . . .	17
2.2	SEM Photograph - Sample 2 . . . . .	17
2.3	PH Stat Apparatus . . . . .	18
2.4	Details of the Batch Reactor . . . . .	19
2.5	Dissolution Rates . . . . .	21
2.6	$K_{sp}$ vs BET Surface Area . . . . .	24
2.7	Crystallization Rates . . . . .	27
3.1	Experimental Apparatus . . . . .	36
3.2	Typical Cumulative Number Distribution Plot . . . . .	39
3.3	Effect of Residence Time . . . . .	43
3.4	Effect of Suspension Density . . . . .	44
3.5	Cumulative Plot with Level Control Problems . . . . .	46
3.6	Effect of pH . . . . .	48
3.7	SEM Photograph - Two Feed System . . . . .	52
3.8	SEM Photograph - Three Feed System . . . . .	52



## List of Tables

Table no.	Title	Page
1.1	Summary of Power Law Expressions . . .	10
2.1	Characteristics of Seed Crystals . . .	16
2.2	Calcium Sulfite Particle Size Distributions . . .	16
2.3	Crystallization Rates . . . . .	29
3.1	Summary of Experimental Data . . . . .	40
3.2	Effect of Gypsum Saturation . . . . .	50
A.1	Channel and Relative Numbers . . . . .	60

## Chapter 1

### Background of Research

#### 1.1 Overview of Flue Gas Desulfurization

Sulfur dioxide into the atmosphere from coal fired power plants is a serious pollution problem. A 1978 U.S. Environmental Protection Agency emissions report states that 64 percent of SO<sub>2</sub> emissions are from coal fired power plants. This contributes to the acid rain problem of forest damage and acidic lakes (Tomlinson, 1983).

Desulfurization of flue gas is used to reduce the SO<sub>2</sub> emissions from power plants. The commercially accepted methods for flue gas desulfurization (FGD) are known as throwaway scrubbing processes. In these processes SO<sub>2</sub> is removed from stack gases with a lime or limestone slurry and CaSO<sub>3</sub>/CaSO<sub>4</sub> solids are produced.

##### 1.1.1 Wet Slurry Scrubbing

Slurry scrubbing is the dominant commercial throwaway process. A simple system is shown in Figure 1.1 (Rochelle and King, 1978). This process reacts lime (CaO) or limestone (CaCO<sub>3</sub>) slurry with the flue gas in the scrubber. CaSO<sub>3</sub>/CaSO<sub>4</sub> solids are precipitated mainly in the crystallizer which is usually a stirred tank. Most of the crystallizer liquid effluent is recycled to the scrubber. The liquid hold-up time is generally between 10 and 20 minutes. This ensures that crystallization occurs in the hold tank and not in the piping and spray headers of the scrubber. A portion of the slurry is withdrawn for liquid/solid separation. This stream contains 5 to 15 weight percent solids with most systems designed to handle 10 weight percent. The solids

residence time varies from 4 to 25 hours. Most systems are designed with solids residence times on the order of 20 hours (Morasky , 1979 and Borgwardt ,1980).

One serious problem of wet slurry scrubbing systems is  $\text{CaSO}_3/\text{CaSO}_4$  scaling in the scrubber. The scrubber feed must not be supersaturated to  $\text{CaSO}_3/\text{CaSO}_4$ . This makes the crystallizer parameters and liquid circulation rates particularly important.

Solid waste disposal is another important problem in throwaway processes. Particle size, shape and sulfate content of the solids effect the dewatering properties of the sludge (Baczek et al., 1986). In particular, calcium sulfite tends to precipitate as rosette shaped crystals in lime systems. Platelets are generally formed in limestone systems (Phillips, 1972). Rosettes are more difficult to dewater than platelets and tend to be unstable in landfills.

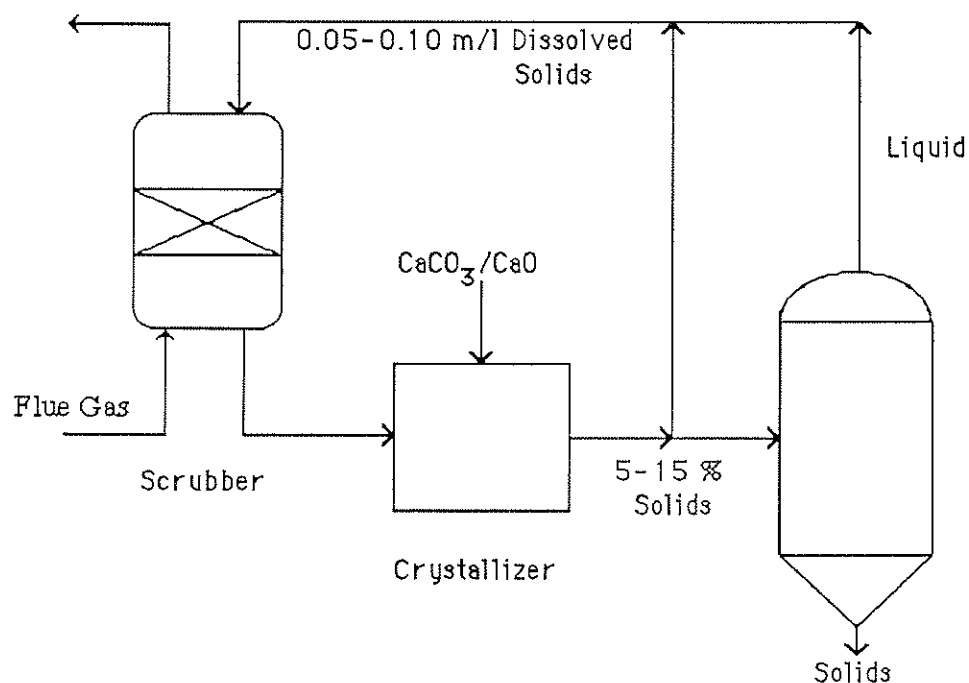


**Figure 1.1.** Simple Slurry Scrubbing

### 1.1.2 Clear Solution Scrubbing

The dual alkali process overcomes the scaling problem of wet slurry scrubbing.  $\text{SO}_2$  is absorbed in a clear solution of sodium sulfite to produce sodium bisulfite. The scrubbing solution is regenerated by lime or limestone to produce  $\text{CaSO}_3/\text{CaSO}_4$  solids. A simple process diagram is shown in Figure 1.2. The solids concentration of the scrubber effluent is 2-5 weight percent. This is lower than the simple lime or limestone slurry processes. The residence time of the solids in the crystallizer is also lower, approximately 100 minutes (Chang et al., 1982).

The solid/liquid separation system is more complex than wet slurry scrubbing. Higher scrubber reliability, higher removal efficiency, and no contaminated liquid effluent are considered major advantages (Cornel and Dahlstrom, 1973).

Recent experience with a limestone dual alkali process showed problems with the build up of fine solids and high oxidation of sulfite to sulfate (Chang and Kaplan, 1983). This resulted in needle-shaped crystals that were difficult to dewater. This was also observed by Simpson and Wilhelm (1985).

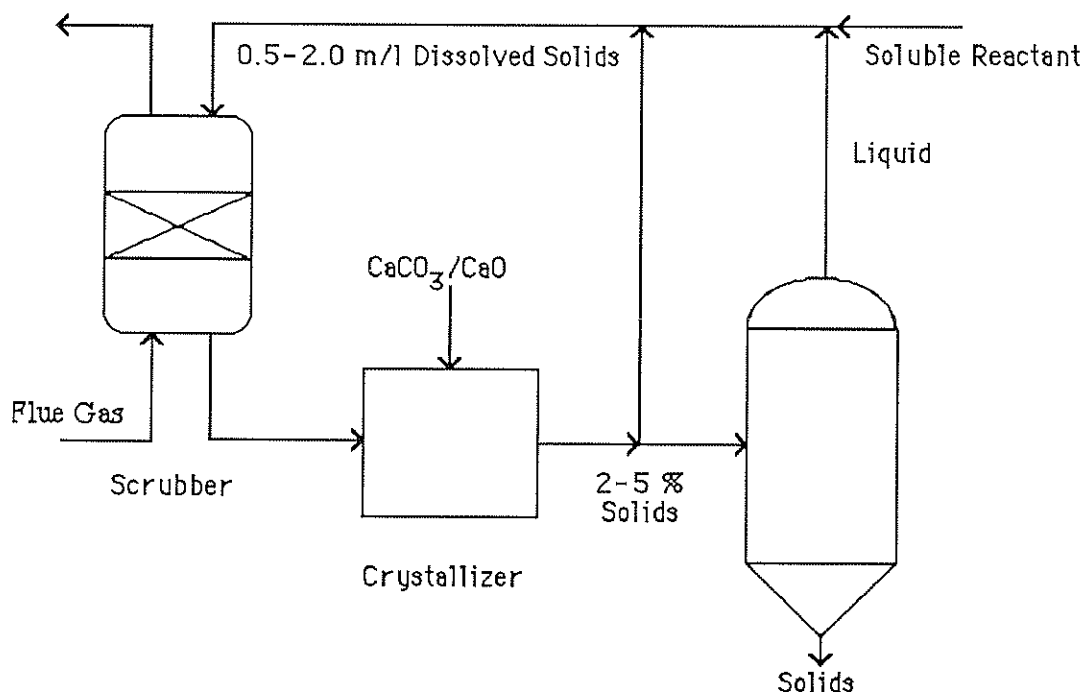


**Figure 1.2. Dual Alkali Process**

### 1.1.3 Spray Drying

Spray drying is a recent development for controlling  $\text{SO}_2$  emissions. It was driven by the desire to obtain a cost effective method of controlling sulfur emissions from low sulfur coal (Doyle and Jankura, 1986). Tests are currently being run to evaluate the feasibility of retrofitting spray dryers at existing power plants that burn medium to high sulfur coal (Brown et al., 1988).

A typical dry scrubbing system is shown in Figure 1.3. A  $\text{Ca}(\text{OH})_2$  slurry is fed to the spray dryer where it is contacted with the hot flue gas.  $\text{SO}_2$  is absorbed by the fine droplets and reacted to form  $\text{CaSO}_3/\text{CaSO}_4$  solids. At the same time the hot flue gas evaporates the water and a dry powder is produced. The dry  $\text{CaSO}_3/\text{CaSO}_4$ , fly ash and unreacted  $\text{Ca}(\text{OH})_2$  are collected by fabric filters or electrostatic precipitators (Reinhauer, 1983 and Rochelle, 1982).

Spray dryer waste consists mainly of fly ash particles (75 weight percent) mixed and coated with  $\text{CaSO}_3/\text{CaSO}_4$  and unreacted  $\text{Ca}(\text{OH})_2$ . The physical and chemical properties of the spray dryer waste are similar to fly ash since fly ash is the major fraction of the waste (Klimek et al., 1986). Particle size and shape of the  $\text{CaSO}_3/\text{CaSO}_4$  solids are not as important in dry scrubbing as they are in wet systems.

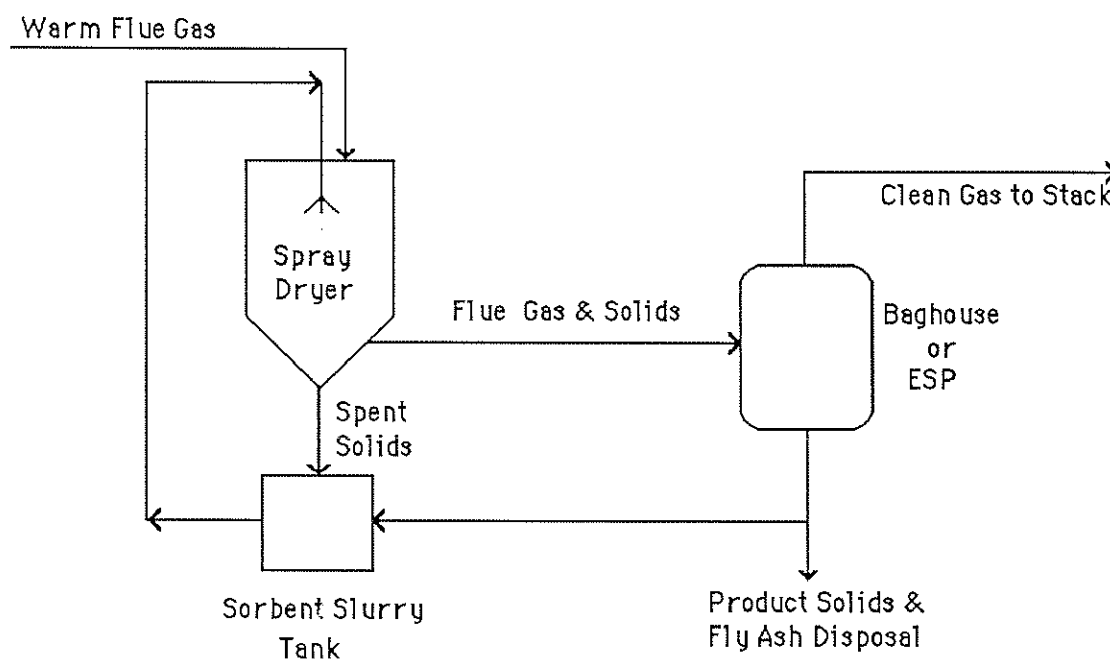


**Figure 1.3.** Spray Drying Process

## 1.2 Previous Work

The dissolution and crystallization of  $\text{CaSO}_3/\text{CaSO}_4$  are important in FGD systems because they effect the scrubber solution composition. Therefore, they can also effect  $\text{SO}_2$  absorption, sulfite oxidation and lime or limestone dissolution (Chan and Rochelle (1982), and Jarvis et al. (1988)). Since stack gases contain oxygen some of the sulfite will be oxidized to sulfate. A mixture of  $\text{CaSO}_3/\text{CaSO}_4$  is obtained as the product. The sulfate content of the solids can effect the crystal size and shape. Crystal size and shape determine the ease of dewatering and thus the economics of waste disposal.

### 1.21 Dissolution and Precipitation

A significant amount of work has been done to characterize and improve the quality of the flue gas scrubber sludge. Philips et al. (1972) evaluated sludges from a limestone and lime scrubbing systems. The limestone sludge contained platelet shaped calcium sulfite hemihydrate crystals. Solids from the lime sludge were rosette shaped. The settled density for the limestone sludge (48 wt. % solids) was greater than that for the lime (34 wt. % solids). This results in easier dewatering of the limestone sludge.

Ottmers et al. (1974) performed experiments to measure the precipitation rate of calcium sulfite. The rate was found to be first order relative to the supersaturation of calcium sulfite. Meserole et al. (1983) determined the effects of high concentrations of dissolved ions on the precipitation of calcium sulfite hemihydrate, gypsum and a solid solution of calcium sulfite/calcium sulfate.

Jones et al. (1976) confirmed the formation of a solid solution of calcium sulfite/calcium sulfate hemihydrate using x-ray diffraction and infra-red spectroscopy. Setoyama and Takahashi (1978) determined that sulfate substitutes for sulfite in calcium sulfite hemihydrate and that the substitution is a function of reaction temperature. The calcium sulfate content in calcium sulfite hemihydrate was 10 wt. % at  $15^\circ\text{C}$  and

increased to 22 wt. % at 83°C. Edwards (1979) performed crystal sizing studies and determined that the crystal size distributions obtained using a Coulter Counter were reliable.

Tseng and Rochelle (1986 a,b) determined the dissolution and crystallization rates of calcium sulfite in aqueous solutions as a function of pH, dissolved sulfite and sulfate, and temperature. The dissolution rate was accurately modeled by assuming the solids are spherical particles in an infinite stagnant solution and accounting for the effect of solution equilibria on the mass transfer driving force. The crystallization rate (correlated with BET surface area rather than size) was found to be second order relative to the calcium sulfite supersaturation. The presence of sulfate in solution reduces both the dissolution and crystallization rates. Several different seed crystals were used in these studies. They varied in sulfate content and crystal habit (agglomerates and rosettes).

### 1.2.2 Nucleation and Crystal Growth

Although there have been numerous studies of the precipitation rate of calcium sulfite, separate nucleation and growth rate information is rare. A recent study by Kelly (1983) measured the growth rate of calcium sulfite. He also performed experiments to determine the effects of various chemical additives on the metastable limit and the crystal habit. Alvarez-Dalama (1986) performed experiments to determine the nucleation and crystal growth rates of calcium sulfite. Also investigated were the effects of high chloride, magnesium, and sodium levels on the crystal habit. Both Alvarez-Dalama and Kelly used a mixed-suspension-mixed-product removal (MSMPR) crystallizer and analyzed the data by the population balance approach. This has the advantage that both nucleation and growth rate determinations can be made at the same time.

Benson et al. (1988) studied calcium sulfite crystallization in the magnesium-lime system. Their laboratory experiments confirmed industrial experience in which



longer residence times and higher solids density resulted in smaller particles. This is the opposite of what occurs in limestone systems. The crystals that form in magnesium-lime systems are rosettes comprised of thin platelets. The rosettes are more susceptible to breakage by agitators and pumps than the thicker platelet crystals formed in limestone systems.

Many other researchers used the population balance approach to study different systems. Randolph and Cise (1972) measured nucleation rates of the potassium sulfate-water system. They correlated their data using a secondary power-law kinetic model and found that the crystal growth rate of potassium sulfate was size dependent.

Grootscholten et al. (1982) studied the effect of impeller type in a MSMPR on the secondary nucleation rate of sodium chloride. They found that a marine propeller gave lower nucleation rates than a pitched blade impeller under identical conditions.

Youngquist and Randolph (1972) found a strong dependence of the stirring rate on the nucleation rate of ammonium sulfate in water. They also found a linear dependence of the nucleation rate on solids concentration. This indicates that nuclei are generated by the collisions of the seed crystals with the impeller blades.

Girolami and Rousseau (1985) studied the potassium alum-water system. They concluded that size-dependent crystal growth is a manifestation of growth rate dispersion. Size-dependent crystal growth occurs when a crystal grows at a different rate when small than when large. Growth rate dispersion occurs when crystals grow at different rates even though they have the same size. These two phenomena are very difficult to distinguish since their effect on the crystal size distribution is the same: higher nuclei population densities and an increase in the spread of the size distribution. Several other studies (Bergland et al. 1982 and 1983, Liang et al. 1986, Garside and Janic 1976) also found nuclei to have a distribution of growth rates but individual crystals to have constant growth rates. Zumstein and Rousseau (1987) developed models including both growth rate dispersion and size dependent growth. The solutions to the population balance for a MSMPR and a batch crystallizer are given.

Gradual classification in continuous crystallizers can also give similar crystal size distributions as growth rate dispersion and size dependent growth. This occurs when residence time for small crystals is less than for large crystals. Bourne and Zabelka (1980) show how the potassium alum - water system behaves when gradual classification occurs due to inadequate mixing.

Impurities can have a appreciable effect on crystallization kinetics and crystal habit. Shor and Larson (1971) studied the effects of various ionic additives and surface active agents on potassium nitrate crystals obtained from a continuous cooling crystallizer. They found some ionic additives increase crystal size while surface active agents decrease crystal size. Peters and Stevens (1982) found that the presence of iron inhibited the growth of calcium carbonate and magnesium hydroxide. Randolph and Puri (1981) studied the sodium tetraborate decahydrate (borax) system. They found that surface active agents inhibited nucleation rates while ionic additives increased nucleation. Both additives decreased the growth rate. Organic additives essentially stopped nucleation at the ppm level. This system is of particular interest since it exhibits classical secondary nucleation behavior.

A variety of crystallization systems have been investigated by many researchers. Table 1.1 is a summary of the power law kinetic expressions that were determined for  $\text{CaSO}_3$  and other compounds. These experiences can be used to analyze  $\text{CaSO}_3/\text{CaSO}_4$  crystallization. Secondary nucleation has been found to be the dominant nucleation mechanism in crystallizers with significant solids concentration. Therefore,  $\text{CaSO}_3/\text{CaSO}_4$  data can be correlated using a power law kinetic expression. Propeller type, level control and adequate mixing are a few important considerations in crystallizer design. Deviations from ideal behavior (size independent growth) must be analyzed carefully since a number of factors can give the same results. Impurities and additives can have a dramatic effect on crystallization kinetics. This can be seen in the kinetic order on the growth rate for the  $\text{CaCO}_3/\text{Mg}(\text{OH})_2$  system (Peters and Stevens, 1982). When iron is present the kinetic order increases from 2.0 to 13.9. This indicates a drastic decrease in the crystal growth rate of  $\text{CaCO}_3$ . Iron poisoned the surface of the crystals and therefore reduced the amount of scale adhering to the reactor walls. Impurities are particularly important in FGD systems where manganese,

magnesium, aluminum, chloride, iron, adipic acid and thiosulfate are a few impurities and additives present.

In general, if the exponent on the growth rate is near 1.0, the particle size distribution does not increase if the solids residence time in the reactor is increased. This is because the quantity  $Gt$  is constant (Randolph, 1971). Also, if the exponent on the solids density ( $M_T$ ) is near one, the shape of the particle size distribution curve is independent of  $M_T$ .

**Table 1.1 Summary of Power Law Expressions: Previous Work**

Compound	Power Law Expression	Reference
CaSO <sub>3</sub> /CaSO <sub>4</sub> in Mg-Lime Systems	$B^0 = K_n G^{0.63} M_T^{2.6}$	Randolph, Benson Wilhelm (1988)
CaSO <sub>3</sub> /CaSO <sub>4</sub> (with Cl <sup>-</sup> ) (with SO <sub>4</sub> <sup>=</sup> )	$B^0 = K_n G^{1.1} M_T^{0.6}$ $B^0 = K_n G^{1.1} M_T^{2.2}$	Alvarez-Dalama (1986)
CaSO <sub>3</sub> /CaSO <sub>4</sub>	$B^0 = K_n G^{0.94} M_T^{1.1}$	Kelly (1983)
CaSO <sub>4</sub> $\frac{1}{2}$ H <sub>2</sub> O	$B^0 = K_n (T) G^{3.19}$	Sikdar, Ore, Moore (1980)
CaSO <sub>4</sub> 2H <sub>2</sub> O	$B^0 = K_n G^{1.48} M_T^{1.27}$	Etherton, Randolph (1981)
CaCO <sub>3</sub> /Mg(OH) <sub>2</sub> (no iron) (with iron)	$B^0 = K_n G^{2.0}$ $B^0 = K_n G^{13.9}$	Peters, Stevens (1982)
Borax	$B^0 = K_n G^{1.48} M_T^{0.84}$	Randolph, Puri (1981)
NH <sub>4</sub> NO <sub>3</sub>	$B^0 = K_n G^{1.22} M_T^{0.98}$	Youngquist Randolph (1972)
NaCl (marine propeller) (pitched blade)	$B^0 = K_n (RPM)^2 G^2 M_T^1$ $B^0 = K_n (RPM)^{2/3} G^2 M_T^1$	Grootscholten, Leer, Dejong (1982)
KCl	$B^0 = K_n (RPM)^k G^{1.67-2.95} M_T^{0.7-1.21}$	Quin et al. (1987)

### **1.3 Scope of Investigation**

There are two major objectives of this work:

- Measure and model the dissolution rate of platelet samples of calcium sulfite hemihydrate at conditions typical of FGD processes.
- Quantify the nucleation and crystal growth of calcium sulfite hemihydrate.

Two platelet samples of  $\text{CaSO}_3/\text{CaSO}_4$  solids were obtained from industrial scrubber systems. These solids were characterized by infra-red spectroscopy, scanning electron microscopy, Coulter Counter particle size analysis and BET surface area measurement. The pH-stat method was used to measure the dissolution, and precipitation rates of the platelet seed crystals. The effects of pH, solution composition and sulfate content of the seed crystals were studied and compared to previous work using agglomerated seed crystals (Tseng, 1986).

The pH-stat apparatus was modified from a semi-batch system to a mixed-suspension-mixed-product-removal (MSMPR) reactor in order to measure the nucleation and crystal growth rates of calcium sulfite hemihydrate. The effects of pH, solution sulfate concentration, solids residence time, solids concentration and temperature on nucleation and growth kinetics were investigated. The product crystals were characterized using scanning electron microscopy, iodine titration, BET surface area (for representative solids only) and Coulter Counter particle size analysis.

## Chapter 2

### Batch Experiments with Platelets

#### 2.1 Summary

The rates of calcium sulfite dissolution and crystallization are important in slurry scrubbing processes for flue gas desulfurization. The rates affect the scrubber solution composition, SO<sub>2</sub> absorption, sulfite oxidation, and limestone utilization. The dissolution and crystallization rates of platelet shaped calcium sulfite crystals were measured in a pH stat apparatus. The solution pH was varied from 3.0 to 6.0. The effects of sulfate content in the solids and solution were also investigated. The measured rates for the platelets were compared to the rates previously determined for agglomerates. It was determined that there are subtle differences between platelet and agglomerated calcium sulfite. The platelet sample with a low solid sulfate content dissolved and crystallized slower than the platelet sample with a high solid sulfate content. Low sulfate platelets also dissolved and crystallized slower than the agglomerated samples. The inhibiting effect of dissolved sulfate was also greater for the sample with low solid sulfate. The sample with high solid sulfate dissolved and crystallized at approximately the same rate as the agglomerates.

#### 2.2 Dissolution

##### 2.2.1 Theory

Calcium sulfite dissolution can be modeled as mass transfer from spherical particles in an infinite stagnant solution. Tseng (1983) discusses in detail the mass

transfer theory and the effects of solution composition and particle size on calcium sulfite dissolution. Briefly, the steady state mass transfer model assumes that chemical equilibrium is maintained for all chemical species in the bulk solution, boundary layer and at the particle surface. The Bechtel-modified-Radian Equilibrium Program (Lowell et al., 1970) was used in the model to calculate the equilibrium constants. The boundary conditions for the model are the solubility product ( $K_{sp}$ ) of calcium sulfite at the particle surface and the specified bulk concentrations. Ionic neutrality and material balances complete the equations that are needed to determine the concentrations of all chemical and ionic species in the boundary layer. The two adjustable parameters in the model are the solubility product ( $K_{sp}$ ) and the Sherwood number (Sh).

The  $K_{sp}$  (Equation 1) is important because it determines the boundary condition at the particle surface.

$$K_{sp} = [a_{Ca^{++}}][a_{SO_3^{=}}] \quad (1)$$

Solids with different sulfate content have different  $K_{sp}$  values. The Sherwood number is a dimensionless group for mass transfer (Equation 2).

$$Sh = \frac{k_c d_p}{D} \quad (2)$$

For small spherical particles in a stagnant solution, the value of the Sherwood number is 2.0. This result is obtained by solving the continuity equation for mass transfer (Chan, 1981). For a single spherical particle the rate of dissolution is given by Equation (3).

$$\frac{dV}{dt} = \frac{Sh \pi d_p (D \Delta C)}{\rho} \quad (3)$$

where  $\Delta C = C - C_s$

The quantity  $D\Delta C$  is calculated from the mass transfer model. Integration of Equation (3) results in the volume fraction remaining of a single particle after time  $t$ . For a given particle size distribution, the total fraction remaining is given by the summation over the particle size distribution (Equation 4).

$$F = \frac{V}{V_0} = \sum \phi_j \left( 1 - \frac{k t}{d_j d_{j+1}} \right)^{1.5} \quad (4)$$

$$\text{where } k = \frac{4ShD\Delta C}{\rho}$$

Deviations of the Sherwood number from 2.0 are due to the presence of large particles, non-spherical particles or to mixing. Rochelle et al. (1983) used a correlation by Calderbank and Moo-Young to model the limestone dissolution rate (Equation 5). Equation 5 is a combination of the stagnant result and an agitation term for larger particles. For large particles the second term dominates the dissolution rate. For small particles the first term (stagnant term) dominates.

$$\frac{dV_p}{dt} = - \frac{\pi \Delta C}{\rho} \left( 2D d_p + 0.13 \left( \frac{\epsilon v}{\rho_c} \right)^{1/4} \left( \frac{D}{v} \right)^{2/3} d_p^2 \right) \quad (5)$$

### 2.2.2 Seed Crystal Characterization

Two samples of calcium sulfite hemihydrate were obtained from industrial scrubbers. Sample 1 was prepared from an industrial sample obtained from Acurex Corporation. It was generated during pilot plant testing in which thiosulfate was used as an additive to inhibit oxidation of sulfite to sulfate. The limestone present in this sample was dissolved in the pH stat apparatus at a calcium sulfite saturation of approximately 1.0. This partially dissolved sample was then grown in the pH stat with the calcium sulfite saturation at approximately 5.0. The results are large single platelet crystals (Figure 2.1)

Sample 2 was obtained from the hold tank of a scrubber from Houston Lighting and Power (June, 1986). The limestone content was very low (2-5 wt. %). The solids were rinsed with distilled water, filtered, and dried. The solids were characterized (Table 2.1) by infrared spectroscopy (IR), scanning electron microscopy (SEM), BET surface area measurement, and particle size analysis (Coulter Counter). Table 2.2 contains the particle size distributions. SEM photographs of the two samples are given in Figures 2.1 and 2.2. Both samples were platelet crystals, but sample 1 was low in sulfate content ( $2.4 \pm 0.5$  mole %) and had a particle thickness of approximately  $5 \mu\text{m}$ . Sample 2 had a high sulfate content ( $15 \pm 0.5$  mole %) and a thickness of less than  $1 \mu\text{m}$ . The median particle diameters for the samples were 16 and  $14 \pm 2 \mu\text{m}$ , respectively. The BET surface area for sample 1 ( $1.0 \pm 0.5 \text{ m}^2/\text{g}$ ) was less than that for sample 2 ( $2.8 \pm 0.2 \text{ m}^2/\text{g}$ ). The error in the BET measurement is larger for the low surface area samples. This is because in nitrogen absorption there is a large error in the equilibrium pressure measurements at low pressures. Also included in Table 2.1 are the characteristics of the agglomerated samples previously studied by Tseng (1983). The  $K_{\text{sp}}$  and the Sherwood number will be discussed later.

### 2.2.3 Experimental Apparatus and Procedure

The dissolution rate of calcium sulfite hemihydrate was determined by the pH stat method. The experimental apparatus was a batch slurry reactor with mechanical stirring and gas sparging (Figure 2.3). Details of the batch reactor are shown in Figure 2.4. It was the same apparatus that was used in previous studies of calcium sulfite dissolution and crystallization (1,4,5). The reactor solution contained 1.0 liter of 0.1 M  $\text{CaCl}_2$ , 10 mM  $\text{Na}_2\text{SO}_3$ , and 2 mM platelet seed crystals. The agitator speed was set at 700 rpms. The reactor was sparged with high purity  $\text{N}_2$  for a half hour before the addition of the calcium sulfite seed crystals. This was done to remove oxygen from the solution in the reactor. The gas sparger was lifted above the solution level to blanket it with  $\text{N}_2$  during the rate measurement. This procedure reduces the oxidation of sulfite to sulfate during the experiment. The pH was automatically controlled to  $\pm 0.02$  units by titrating with 0.02 to 0.2 M  $\text{Na}_2\text{SO}_3$ . The experiments were performed at room temperature.



**Table 2.1** Characteristics of Seed Crystals, Adjusted Sherwood Number and  $K_{sp}$  of Calcium Sulfite (0.1 M  $\text{CaCl}_2$ , 10 mM  $\text{Na}_2\text{SO}_3$ , 23°C)

Crystal Habit	Platelets		Agglomerates (4,5)		
Sample No.	1	2	Seed 1	Seed 3	Seed 5
$\text{CaSO}_4$ Content ( $\pm 0.5$ mole %)	2.4	15	3.4	10.7	1.0
BET Surface Area ( $\text{m}^2/\text{g}$ )	$1.0 \pm 0.5$	$2.8 \pm 0.2$	$1.9 \pm 0.3$	$9.5 \pm 0.1$	$1.2 \pm 0.5$
Median Size ( $\pm 2.0 \mu\text{m}$ )	16	14	16	13	18
$K_{sp} \times 10^7$ (no sulfate) ( $\text{M}^2$ )	$1.6 \pm 0.2$	$3.2 \pm 0.4$	$2.7 \pm 0.4$	$3.4 \pm 0.4$	$2.4 \pm 0.4$
Sh (no sulfate) ( $\pm 0.1$ )	2.0	3.8	3.4	3.8	4.0
$K_{sp} \times 10^7$ (10 mM sulfate) ( $\text{M}^2$ )	$2.2 \pm 0.3$	$3.4 \pm 0.4$	-	-	-
Sh (10mM sulfate) ( $\pm 0.1$ )	0.3	1.4	-	-	-

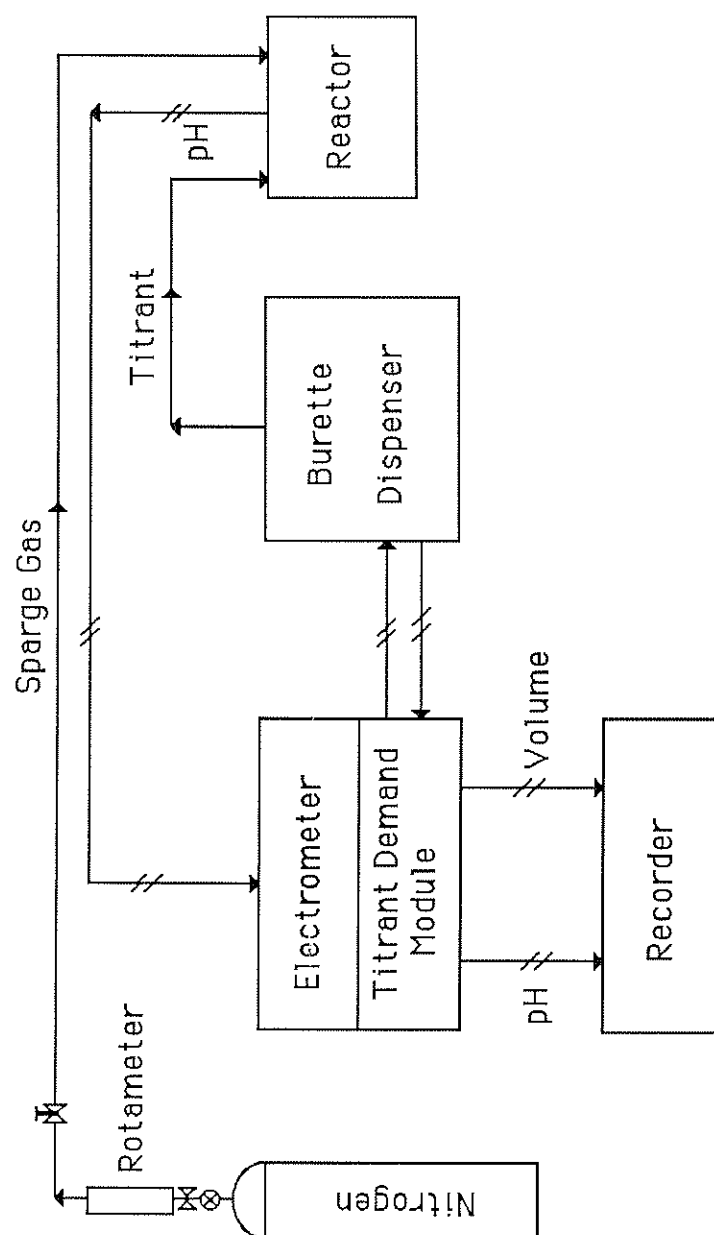
**Table 2.2** Calcium Sulfite Particle Size Distributions

Coulter Counter TAPII (Electrolyte: 4 wt%  $\text{CaCl}_2$ , 140, 200, and 400  $\mu\text{m}$  apertures)

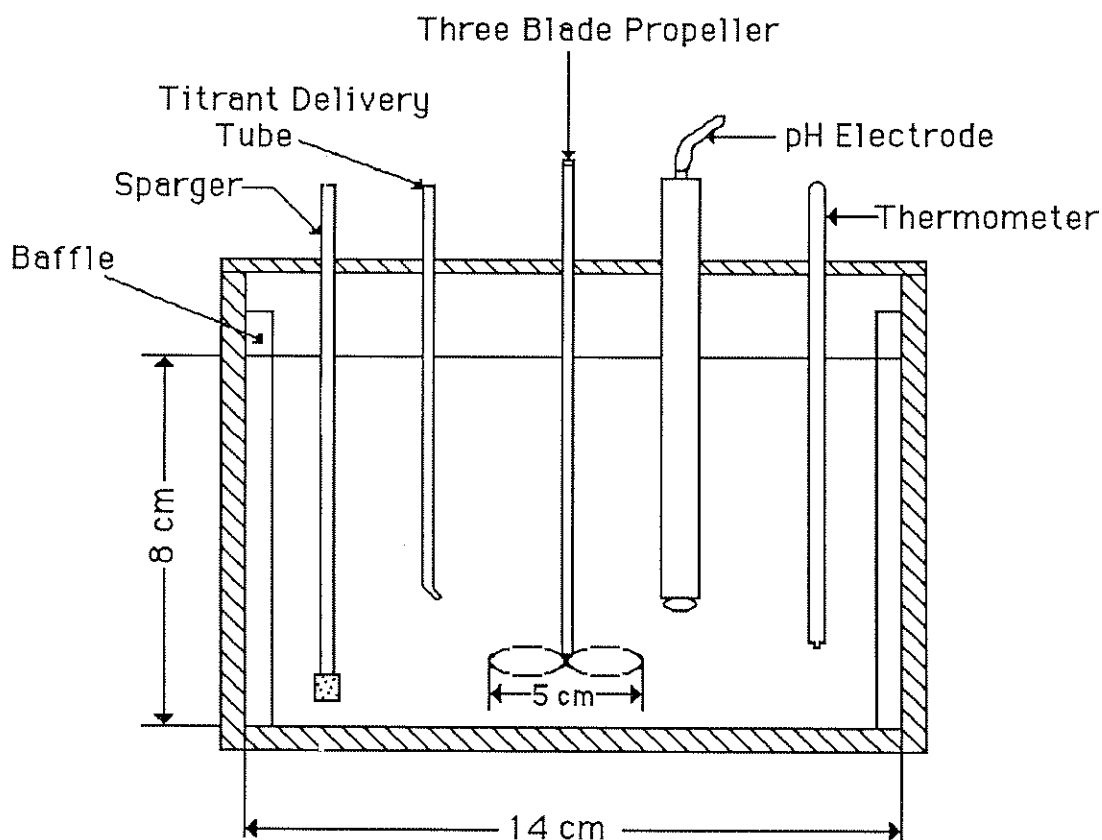
Effective Diameter-lower limit ( $\mu\text{m}$ )	CaSO <sub>3</sub> Volume Percent Sample Number	
	1	2
1.56		0.1
2.00		0.6
3.17		1.0
4.00	1.8	2.3
5.04	2.8	3.9
6.35	4.7	5.4
8.00	7.5	9.5
10.08	11.9	12.2
12.7	15.2	14.1
16.0	16.4	14.9
20.2	15.0	11.7
25.4	11.3	9.7
32.0	6.9	5.6
40.3	3.4	3.8
50.8	2.0	1.7
64.0	0.9	1.5
80.6	0.2	0.7
101.6		0.8
128.0		0.3

Figure 2.1 SEM Photograph of Sample 1  
Magnification 540X

Figure 2.2 SEM Photograph of Sample 2  
Magnification 600X



**Figure 2.3 pH Stat Apparatus**



**Figure 2.4** Details of the Batch Reactor

As calcium sulfite dissolves, the pH increases. To keep the pH constant, HCl was added to the reactor according to Equation (6).



The HCl titration rate is not exactly equal to the calcium sulfite dissolution rate. There is an equilibrium relationship which must be included (Equations 7,8).



$$\text{moles CaSO}_3 \text{ dissolved} = \text{moles HCl added} \frac{1+K_a[H^+]}{K_a[H^+]} \quad (8)$$

The equilibrium constant  $K_a$  used in the rate calculation was determined experimentally by Tseng (1983) and has the value  $1.1 \times 10^{-6} \text{ M}^2$  in 0.1 M  $\text{CaCl}_2$  at  $25^\circ\text{C}$ .

In a dissolution experiment the fraction remaining,  $F$ , can be calculated from the volume of HCl titrated as a function of time. With a numerical solution of Equation (4), the value of  $kt$  can be calculated as a function of the fraction remaining and the initial particle size distribution,  $\phi_j$ . The time interval for 45 to 55 percent of the solids to dissolve is measured. Then the experimental rate constant can be determined from Equation (9).

$$k = \frac{(kt)_{55} - (kt)_{45}}{t_{55} - t_{45}} \quad (9)$$

#### 2.2.4 Results and Discussion

The calcium sulfite hemihydrate dissolution rates were measured for platelet seed crystals with different sulfate contents. The pH was varied from 3.5 to 4.2 in 0.1 M  $\text{CaCl}_2$  and 10 mM  $\text{Na}_2\text{SO}_3$ . With the large amount of  $\text{Ca}^{++}$  in solution, the calcium concentration did not change significantly during the dissolution experiment. The sulfite and sulfate concentrations were the important factors. The results are compared to previous work by Tseng (1986) in which the seed crystals were agglomerates.

##### 2.2.4.1 Effects of Particle Size/Shape and Sulfate Content in the Solids

The dissolution rate constant is plotted as a function of pH for the two platelet samples in Figure 2-5. The curves given in Figure 2-5 were calculated by the stagnant solution mass transfer model. The Sherwood number ( $Sh$ ) and the solubility product ( $K_{sp}$ ) were adjusted to give the best fit of the model for each seed crystal and each

sulfate solution concentration (Table 2-1). First the Sherwood number was determined. Changes in the Sherwood number affect the vertical placement of the curve. Then the  $K_{sp}$  was determined. The  $K_{sp}$  affects the equilibrium pH and therefore where the slope of the curve approaches infinity. The general shape of the curve is not affected by reasonable values of  $K_{sp}$  and  $Sh$ . Therefore, once the endpoints were fixed, intermediate predicted values of the rate constant and the experimental values were close.

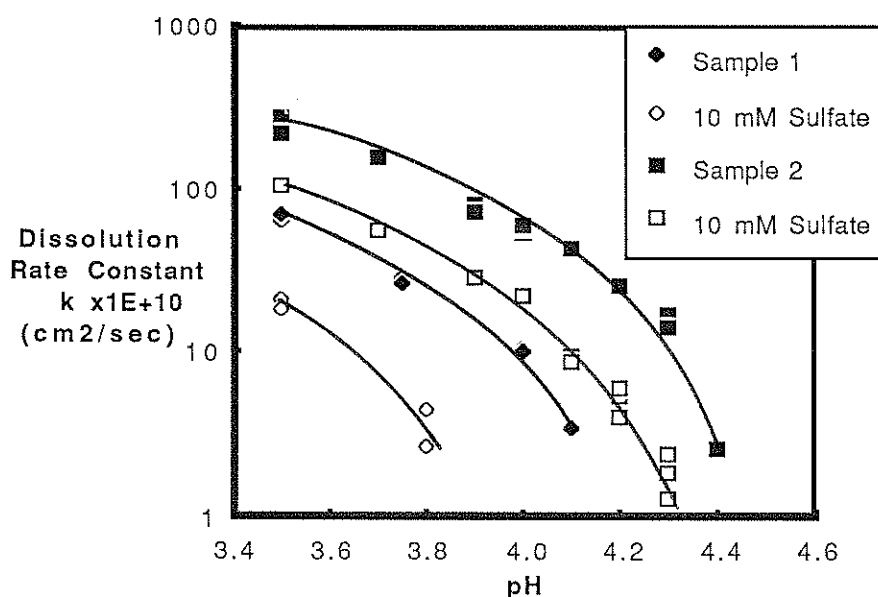


**Figure 2.5** Effects of Solid and Dissolved Sulfate Content on Calcium Sulfite Dissolution Rates and Equilibrium pH.  
(0.1M  $\text{CaCl}_2$ , 10mM  $\text{Na}_2\text{SO}_3$ , 23°C  
Curves Calculated by the mass transfer model)

For a given  $K_{sp}$ , the predicted rate is directly proportional to the Sherwood number. For example, the low sulfate platelet sample 1 has a measured dissolution rate of  $6.6 \pm 0.2 \times 10^{-9} \text{ cm}^2/\text{sec}$  (at pH 3.5). A Sherwood number of 2.0 and  $K_{sp}$  of  $2.2 \times 10^{-7}$

$M^2$  results in a predicted rate constant of  $6.5 \times 10^{-9} \text{ cm}^2/\text{sec}$  at pH 3.5. A  $\pm 0.1$  (5%) change in the Sherwood number results in a  $\pm 0.4 \times 10^{-10}$  (6%)  $\text{cm}^2/\text{sec}$  change in the predicted dissolution rate constant. This change in the rate constant is approximately the same as the experimental error. At pH values greater than 0.5 pH units below the equilibrium pH, the predicted rate is insensitive to the value of the  $K_{sp}$ . Therefore, the reported values of the Sherwood number should be good within  $\pm 5$  percent.

Near equilibrium, the dissolution rate is very sensitive to the  $K_{sp}$ . The confidence in the value of the  $K_{sp}$  is related to the accuracy in the measured value of the pH. With the pH measurement good to  $\pm 0.05$ , the  $K_{sp}$  is accurate within  $\pm 12$  percent. For example, the low sulfate platelet sample 1 has a measured dissolution rate of  $3.5 \pm 0.2 \times 10^{-10} \text{ cm}^2/\text{sec}$  (at pH 4.1). A Sherwood number of 2.0 and  $K_{sp}$  of  $2.2 \times 10^{-7} M^2$  results in a predicted rate constant of  $3.6 \times 10^{-9} \text{ cm}^2/\text{sec}$  at pH 4.1. A  $\pm 0.2 \times 10^{-7}$  (10%) change in the  $K_{sp}$  results in a  $\pm 0.5 \times 10^{-10}$  (15%)  $\text{cm}^2/\text{sec}$  change in the predicted dissolution rate constant. This change in the rate constant is approximately the experimental error.

The dissolution rate appears to be affected by both particle shape and the sulfate content of the solids. The low sulfate platelets (sample 1) dissolved slower than the other two samples and had the lowest equilibrium pH. The high sulfate platelets (sample 2) dissolved at approximately the same rate as the agglomerated samples, but sample 2 had a slightly higher equilibrium pH than the agglomerates. This is reflected in the values of the Sherwood number and  $K_{sp}$  determined for each seed crystal. The Sherwood number reflects the changes in agitation, particle size and shape. In these experiments the Sherwood numbers for thin platelets (sample 2) and agglomerates are 3.4 to 4.0. Large non-spherical particles and mixing can cause the Sherwood number to be higher. Rochelle et al. (1983) used the Calderbank and Moo-Young expression (Equation 5) to predict limestone dissolution rates. Equation 5 can be rewritten as

$$\frac{dV_p}{dt} = -KV_p^{1/3}[1 + BV_p^{1/3}] \quad (10)$$

where

$$K = 6^{1/3} \text{ Sh} D \Delta C \pi^{2/3} / \rho$$

$$B = \frac{0.0807 (\epsilon v)}{D} \left( \frac{D}{\rho_c} \right)^{1/4} \left( \frac{D}{v} \right)^{2/3}$$

Equation (10) can be set equal to the stagnant dissolution rate expression (Equation 3) with the definition of the experimental rate constant substituted into Equation 3. The result is Equation (11).

$$\frac{k\pi d}{4} = K[V_p^{1/3} + B V_p^{2/3}] \quad (11)$$

Substitution for K and solving for the Sherwood number results in Equation (12).

$$\text{Sh} = \frac{k\rho}{D \Delta C (1 + B V_p^{1/3})} \quad (12)$$

The value of B was experimentally determined by Rochelle et al., (1983) to be 0.04 micron<sup>-1</sup> for a similar reactor set up with similar agitation as Figure 2.4. Typical values of D ΔC and k and an average particle size of 15 microns are listed below.

$$\begin{aligned} \rho &= 0.0194 \text{ mole/cm}^3 \text{ for calcium sulfite hemihydrate} \\ k &= 5.0 \times 10^{-9} \text{ cm}^2/\text{sec} \\ D \Delta C &= 2 \times 10^{-8} \frac{\text{gmole-cm}^2}{\text{liter-sec}} \end{aligned}$$

The Sherwood number calculated from Equation (12) is 2.6. Therefore agitation and larger particles account for a significant extent for the higher Sherwood number.

The value of the  $K_{sp}$  determined for each seed crystal appears to be dependent on the solids BET surface area. Figure 2.6 is a plot of the  $K_{sp}$  as a function of the BET surface area. The  $K_{sp}$  increased as the BET surface area of the solids increased. This is the direction one expects the  $K_{sp}$  to change as a result of surface energy interactions between liquid and solid.



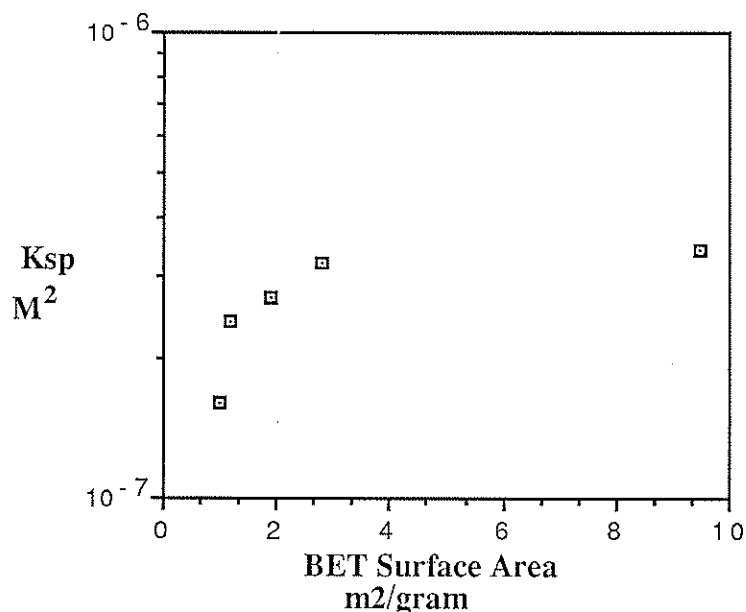


**Figure 2.6** Solubility Product (K<sub>sp</sub>) of Calcium Sulfite as a Function of BET Surface Area

#### 2.2.4.2 Effects of Dissolved Sulfate

The effects of sulfate were determined by adding 10 mM Na<sub>2</sub>SO<sub>4</sub> to the reactor solution. This corresponds to a gypsum saturation of 1.0 (12). Figure 2.5 is a plot of the experimental rate constant as a function of pH. The presence of sulfate inhibits the dissolution rate of platelet calcium sulfite at low and high values of pH. Tseng (1986) found that sulfate in solution also inhibited the dissolution rate of agglomerated calcium sulfite. The amount that the rate decreased is approximately the same for sample 2 and the agglomerates. Sulfate in solution has a slightly greater inhibiting effect on sample 1 with low sulfate and low surface area.

The mass transfer model can be used to model these results by reducing the Sherwood number and K<sub>sp</sub> (Table 2.1). This suggests that dissolution of calcium sulfite in the presence of sulfate is still mass transfer controlled, but the effective area for dissolution is reduced (Tseng, 1986). The sulfate ions may adsorb onto the large

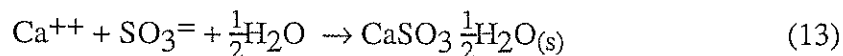
faces of the crystals which would leave only the edges available for dissolution. This would result in slower dissolution rates in the presence of sulfate and also slower dissolution rates for platelets than agglomerates.

## **2.3 Crystallization**

### **2.3.1 Experimental Apparatus and Procedure**

The crystallization rate of calcium sulfite crystals was also determined by the pH stat method. The agitator speed was set at 450 rpm. The reactor solution (0.1 M  $\text{CaCl}_2$ , 10 mM  $\text{Na}_2\text{SO}_3$ , and 1 mM platelet seed crystals) was sparged and blanketed with  $\text{N}_2$  in the same manner as in the dissolution experiments. The experiments were performed at room temperature.

When calcium sulfite crystallizes,  $\text{SO}_3^{=}$  is consumed according to Equation (13).



This causes  $\text{H}^+$  to be released into solution to maintain the equilibrium relationship between  $\text{SO}_3^{=}$  and  $\text{HSO}_3^-$  (Equation 7).

This pH drop causes the pH stat to dispense  $\text{Na}_2\text{SO}_3$  to maintain the pH at the original value. Therefore the crystallization rate of calcium sulfite is equal to the titration rate of  $\text{Na}_2\text{SO}_3$ . The crystallization rate was determined when the concentration of solid calcium sulfite had doubled to 2mM. This rate was then normalized by the BET surface area of the initial seed.

The crystallization rate was correlated as a function of calcium sulfite relative supersaturation. Supersaturations were calculated by the Bechtel-modified Radian Equilibrium Program (Lowell et al., 1970). The relative saturation is defined by:

$$RS_{CaSO_3} = \frac{a_{Ca^{++}} a_{SO_3^{=}}}{K_{sp}} \quad (14)$$

The value of the  $K_{sp}$  used in the correlation was based on the  $K_{sp}$  determined in the dissolution experiments.

### 2.3.2 Results and Discussion

The calcium sulfite crystallization rates were measured for platelet seed crystals with different sulfate contents. The solution pH was varied from 4.7 to 6.0 in 0.1 M  $CaCl_2$  and 10mM  $Na_2SO_3$ . This corresponds to a calcium sulfite relative saturation of approximately 2 to 15. Sulfate was added to the reactor solution at pH 5.25 to quantify the inhibiting effect of sulfate on platelet calcium sulfite. The results are compared with previous work by Tseng (5) in which the seed crystals were agglomerates.

#### 2.3.2.1 Crystallization Rate Correlation

Tseng (1986) found that the crystallization rate of agglomerate seed crystals was second order relative to the supersaturation of calcium sulfite and inversely proportional to gypsum saturation (Equation 15). The crystallization rate is normalized by the BET surface area of the solids. With that representation, the magnitude of the crystallization rate for platelets is comparable to agglomerates.

$$R \left( \frac{\text{mole}}{\text{min-cm}^2} \right) = 9.7 \times 10^{-4} e^{(-10 \times 10^3 / RT)} \frac{[RS_{CaSO_3} - 1]^2}{RS_{CaSO_4}} \quad (15)$$

The gypsum saturation was taken to be 0.025 when no sulfate was added to the reactor.

Figure 2.7 is a plot of the crystallization rate as a function of relative supersaturation for the two platelet seed crystals and the agglomerates previously studied by Tseng. The order of calcium sulfite supersaturation dependence is  $3.0 \pm 0.3$  and  $2.8 \pm 0.2$  for platelet samples 1 and 2, respectively. The high sulfate platelets appear to crystallize faster than either agglomerates or low sulfate platelets. Data taken

at calcium sulfite relative saturations higher than 10 were excluded from this analysis. At high saturations the crystallization rate was very fast. Nucleation and crystal growth occurred before the seed crystals could be added to the reactor. This is higher than the second order dependence determined by Tseng(1986). However, if only the data at low supersaturations is analyzed, the order is closer to 2 which is in agreement with Tseng.

The dependence of the growth rate on the supersaturation from these semi-batch experiments can be used in Chapter 3 (continuous experiments) to predict the nucleation rate as a function of supersaturation (see Section 3.4.5). Since continuous crystallizers operate at supersaturations very close to zero, a second order dependence will probably predict nucleation rates more accurately.

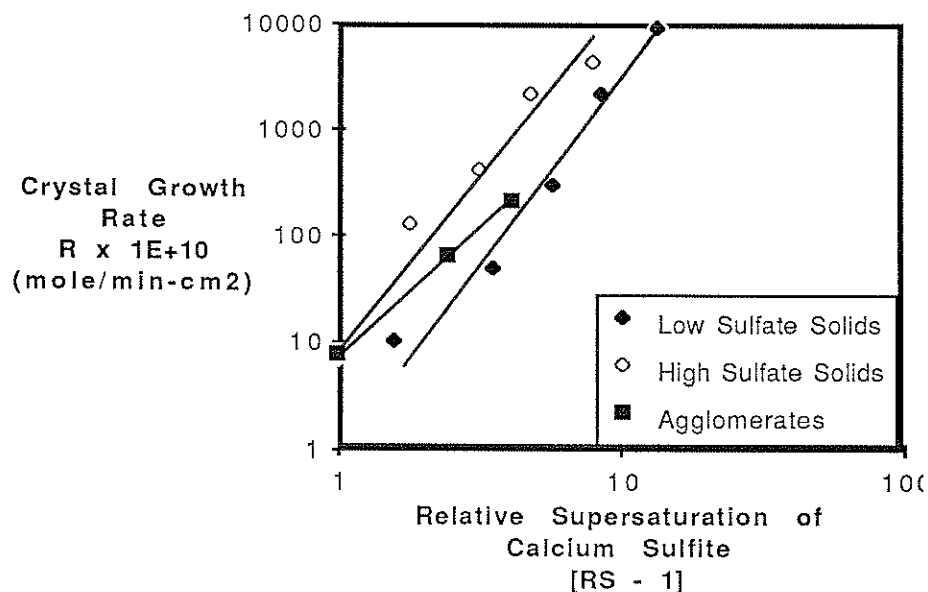


**Figure 2.7** Calcium Sulfite Crystallization Rate  
(0.1M CaCl<sub>2</sub>, 10mM Na<sub>2</sub>SO<sub>3</sub>, 23°C)

### 2.3.2.2 Effect of Gypsum Saturation

The effect of dissolved sulfate on the crystallization rate of platelet calcium sulfite was determined by varying the gypsum saturation from 0.025 to 2.0 at a set pH (5.25). Table 2.3 is a summary of these results. The crystallization rate decreased as the dissolved sulfate increased for the low sulfate platelets (sample 1).

Tseng (1983b) found that crystallization rate was inversely proportional to gypsum saturation. Correlation of sample 1 data results in a slightly higher sulfate dependence,  $-1.4 \pm 0.3$  (Equation 12). Again, if only the lower saturations are used to determine the order, the value is closer to one which is in agreement with Tseng.

$$\text{Rate} \propto (\text{RSCaSO}_4)^{-1.4} \quad (16)$$

The higher order could be due to the sulfate ions adsorbed onto the large faces of the crystals. This would leave only the edges available for crystal growth and result in slower crystallization rates in the presence of sulfate. Also, platelets would crystallize slower than agglomerates.

**Table 2-3.** Effects of Gypsum Saturation on the Crystallization Rate of Calcium Sulfite Seed Crystals  
(0.1 M CaCl<sub>2</sub>, 10 mM Na<sub>2</sub>SO<sub>3</sub>, pH 5.25, 23°C)

Seed Crystal	RS <sub>CaSO<sub>3</sub></sub>	RS <sub>CaSO<sub>4</sub></sub>	Rate (moles/min-cm <sup>2</sup> )
Sample 1	6.8	0.025	3.1 x 10 <sup>-8</sup>
Low Sulfate	6.7	0.5	8.6 x 10 <sup>-9</sup>
Platelets	6.5	1.0	6.4 x 10 <sup>-9</sup>
	6.3	2.0	1.2 x 10 <sup>-9</sup>
Sample 2	4.3	0.025	4.0 x 10 <sup>-8</sup>
High Sulfate	4.1	0.5	3.0 x 10 <sup>-9</sup>
Platelets			
Agglomerates	5.2	0.025	2.0 x 10 <sup>-8</sup>
Seed 1	4.8	1.9	6.1 x 10 <sup>-9</sup>

## 2.4 Nomenclature

a	activity (M)
C	solute concentration in bulk liquid (M)
C <sub>s</sub>	solute concentration at particle surface (M)
d <sub>p</sub>	particle diameter (cm)
D	Ca++ diffusivity (cm <sup>2</sup> /sec)
F	total fraction of particles remaining
k	dissolution rate constant (cm <sup>2</sup> /sec)
k <sub>c</sub>	mass transfer coefficient (cm/sec)
K <sub>a</sub>	equilibrium constant
K <sub>sp</sub>	calcium sulfite solubility product (M <sup>2</sup> )
M	molarity (mole/liter)
R	crystallization rate based on BET surface area (mole/min-cm <sup>2</sup> )
RS	relative saturation
Sh	Sherwood number
t	time (sec)
T	temperature (K)
V	volume of single particle (cm <sup>3</sup> )
V <sub>T</sub>	total volume of particles (cm <sup>3</sup> )
V <sub>0</sub>	total initial volume of particles (cm <sup>3</sup> )

### Greek Symbols

e	agitation power per gram solution (cm <sup>2</sup> /sec <sup>3</sup> )
ρ <sub>c</sub>	density of solution (gm/cm <sup>3</sup> )
ν	kinematic viscosity of solution (cm <sup>2</sup> /sec)
ρ	crystal density (0.0194 mole/cm <sup>3</sup> )
ø <sub>j</sub>	fraction of total particle volume with diameters from d <sub>j</sub> to d <sub>j+1</sub>

## Chapter 3

### Nucleation and Crystal Growth

#### 3.1 Summary

Sludge disposal is a significant cost in most slurry scrubbing processes for flue gas desulfurization. The settling rate and settled density of the sludge are related to the particle size distribution of the calcium sulfite particles. Size distributions can be predicted if nucleation and growth rates are known. These rates can also be used to examine prospects for increasing the calcium sulfite particle size. This would lead to an improved sludge quality and lower disposal costs.

The nucleation and crystal growth rates of calcium sulfite hemihydrate were measured in a continuous flow crystallizer. The effects of solution sulfate concentration, residence time, suspension density and temperature on the rates were investigated. It was determined that the nucleation rate was directly proportional to the suspension density. The particle size distribution does not change when the suspension density is changed. The growth rate was found to be directly proportional to the solids residence time in the reactor. Therefore, particle size distribution cannot be increased by increasing the residence time in the reactor. The activation energy for  $\text{CaSO}_3 \cdot \frac{1}{2}\text{H}_2\text{O}$  nucleation was estimated to be 4 kcal/mole within the temperature range of 25 to 55 °C. The nucleation rate constant increased over the pH range of 4.5 to 5.5. Sulfate in solution caused the nucleation rate to decrease.



### 3.2 Theory

There are two major processes in crystallization:

1. Nucleation (new crystal formation)
2. Crystal growth

The driving force for both of these processes is the liquid supersaturation. Crystal growth occurs at low levels of supersaturation, but nucleation does not (Kelly, 1983 and Otters et al., 1974). Sometimes nucleation will not occur unless seed are introduced (Strickland-Constable, 1980). Consequentially, for a quantitative study of crystallization, nucleation and growth must be considered distinct phenomena.

#### 3.2.1 Nucleation

There are three mechanisms of nucleation:

1. Homogeneous - formation of new crystals due to only the liquid supersaturation.
2. Heterogeneous - formation of new crystals due to the presence of foreign insoluble material.
3. Secondary - formation of new crystals in the presence of the same type of crystals.

In industrial crystallizers, secondary nucleation is the most important mechanism. Clontz and McCabe (1971) demonstrated that contact energy and supersaturation are important factors in new crystal formation. An empirical power law expression has been found to adequately predict the nucleation rate ( $B^0$ ) for most secondary systems. Equation 1 is the power law equation which shows that the nucleation rate is a function of the suspension density ( $M_T$ ) and supersaturation ( $s$ ).

$$B^0 = k_n M_T^{i,j} s^j \quad (1)$$

### 3.2.2 Crystal Growth

Crystal growth can be characterized by a three-step mechanism:

1. Diffusion of solute to the crystal surface.
2. Adsorption of the solute onto the crystal surface.
3. Integration of solute into the crystal lattice.

In a stagnant solution the linear crystal growth rate ( $G$ ) is usually limited by the diffusion rate and therefore proportional to the supersaturation ( $s$ ).

$$G = \frac{dL}{dt} = ks \quad (2)$$

For agitated solutions the surface integration step usually controls. Burton, et al., (1951) state that growth along screw dislocations is the most probable. This is represented by:

$$G = ks^2 \quad (3)$$

Other mechanisms have been proposed such as the spiral growth mechanism by Van Rosmalen (1981) for low values of supersaturation. He also stated that for high supersaturations growth may be due to polynuclear surface nucleation. These mechanisms can not be related to a second order function of supersaturation. To account for the variety of growth mechanisms a power-law type expression is used (Equation 4). Values of ( $a$ ) range from one to two.

$$G = ks^a \quad (4)$$

The growth rate expression can be used to eliminate the supersaturation term in the power law expression (Equation 5).

$$B^0 = k_n M_T^i G^j \quad (5)$$

### 3.2.3 Population Balance

The crystallization process can be described in terms of a population balance. It accounts for particles entering and leaving the system, and growth and breakage of existing particles. The population balance for a system as derived by Randolph and Larson (1971) is shown in Equation (6).

$$\frac{\partial n}{\partial t} + \frac{\partial(Gn)}{\partial L} + D - B + \frac{nd(\ln V)}{dt} = - \sum_k \frac{n_k Q_k}{V} \quad (6)$$

For a steady state system where breakage is negligible, and there are no particles in the inlet streams, Equation 6 reduces to:

$$\frac{\partial Gn}{\partial L} + \frac{nQ}{V} = 0 \quad (7)$$

When the growth rate is independent of crystal size (McCabe's  $\Delta L$  Law, 1929) Equation (7) can be easily integrated to:

$$n = n^0 \exp\left(-\frac{L}{G\tau}\right) \quad (8)$$

Substitution of the definition of the population density (Equation 9) into Equation (8) and integration from size  $L$  to infinity results in an expression for the cumulative size distribution (Equation 10).

$$n = \frac{dN}{dL} \quad (9)$$

$$N_L = n^0 G \tau \exp\left(-\frac{L}{G\tau}\right) \quad (10)$$

A plot of  $\ln N_L$  versus  $L$  should result in a straight line with an intercept of  $\ln(n^0 G \tau)$  and slope of  $-\frac{L}{G \tau}$ . The nucleation rate can be determined from Equation (11).

$$B^0 = \left( \frac{dN(L)}{dt} \right)_{L \rightarrow 0} = \left( \frac{dN(L)}{dL} \right)_{L \rightarrow 0} \left( \frac{dL}{dt} \right) = n^0 G \quad (11)$$

### 3.3 Experimental Apparatus and Procedure

The pH-stat apparatus was modified from a semi-batch system to a continuous mixed-suspension-mixed-product-removal (MSMPR) reactor in order to measure the nucleation and crystal growth rates of calcium sulfite hemihydrate (Figure 3.1). It consisted of a jacketed, 500 ml agitated reactor with nitrogen sparging. The lid was a rubber stopper (4 cm thick) that fitted tightly in the reactor. There were holes drilled into the stopper for the agitator, thermometer, feed streams (5 cm apart), pH electrode and titrant delivery tube. The agitator was a three blade marine-type propeller. The two feed streams ( $\text{CaCl}_2$  and  $\text{Na}_2\text{SO}_3/\text{Na}_2\text{SO}_4$  mix) were fed by a dual head MasterFlex peristaltic pump with a 10 turn potentiometer speed control. The motor speed range was 1 to 100 rpm. Size 13 tubing was used which corresponds to feed flow rates from 0.5 ml/min to 7 ml/min. All feed streams are fed below the liquid level. Fine tuning of the reactor pH was done with the pH stat apparatus using 1.0 M HCl as the titrant. Titrant delivery was also below the liquid level.

Level control was also achieved with a MasterFlex peristaltic pump with size 16 tubing. The end of the tubing was cut at a slant and a small hole (0.5 cm in diameter) was cut 1 cm above the slant. The level control tubing was placed in the reactor with the small hole at the desired liquid level. This was done to ensure that the contents of the exit stream were the same as the contents of the reactor. The peristaltic pump was set to pump at 25 ml/min.

Prior to all experiments the agitator and peristaltic pumps were calibrated. All experiments were performed with an agitator speed of 370 rpm. Higher speeds caused

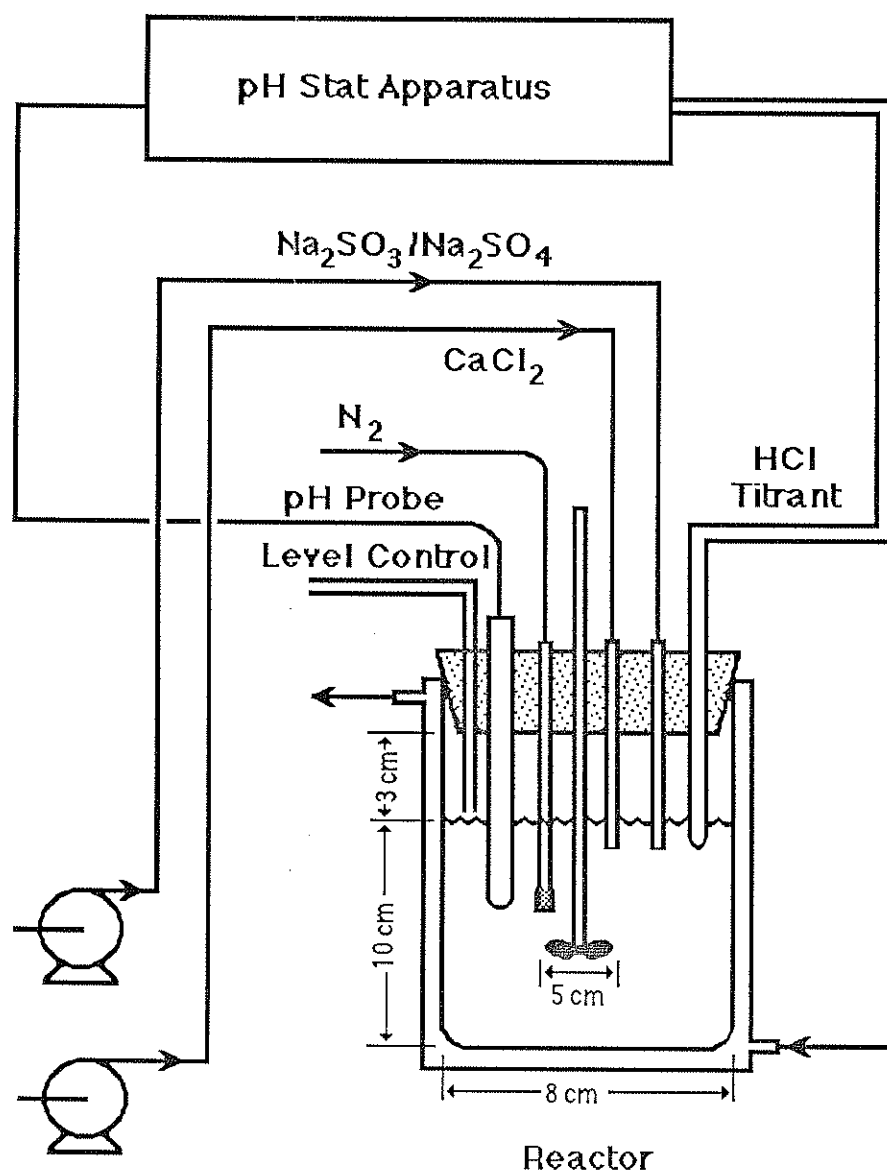


**Figure 3.1.** Experimental Apparatus

the liquid level to vortex around the agitator shaft. Lower rpms did not produce adequate mixing.

Initially, the reactor was filled with 500 ml of 0.1 M  $\text{CaCl}_2$  solution. This was sparged with oxygen free nitrogen for approximately one-half hour while heating up to the desired temperature ( $55^\circ\text{C}$ ). The pH electrode was calibrated at the reactor temperature with a pH 7 buffer (potassium phosphate monobasic (0.05M) - sodium hydroxide and a pH 5 buffer (adipic acid (0.005M) - sodium hydroxide, in 0.1M calcium chloride) . Then 3-5 ml of 0.5M  $\text{Na}_2\text{SO}_3$  was added to the reactor and the pH was adjusted to the desired value. The feed and level control pumps were started and the pH stat apparatus turned on.

During each experiment the reactor pH and titrant demand were recorded on a strip chart recorder. The flow rate of the exit stream was also monitored using a graduated cylinder and stop watch method several times during the experiment. The experiment was allowed to run for 6-7 residence times before slurry samples were taken for analysis.

Approximately 40 ml of slurry was removed from the reactor with the level control tubing immersed in the reactor. Ten mls of this slurry was filtered with a 0.5 micron Millex filter unit. The clear solution was immediately placed in a small sample vial and capped. It was later (within 15 minutes) analyzed for total sulfite content using iodine titration (Appendix A). One ml of the slurry sample was placed in 200 ml of 4 weight percent  $\text{CaCl}_2$  (filtered to 0.5 microns) for analysis in a Coulter Counter TAIL using a 400 micron aperture. The number of particles per ml and the particle size distribution of the slurry were measured. Details of the Coulter Counter method are in Appendix A. Slurry samples were taken 2-4 times before the experiment ended at approximately 11 residence times. The contents of the reactor were vacuum filtered, rinsed with approximately 100 ml of distilled water, vacuum dried at  $80^\circ\text{C}$ , weighed and saved for later analysis.

It was found that after approximately seven residence times the number of particles per ml ( $N_T$ ) varied  $\pm 10$  percent. The particle size distribution was also

constant after seven residence times (each channel was  $\pm 10$  percent of its previous value). This was the experimental error of the Coulter Counter measurement. The experiment was considered to be at steady state when 2-3 successive samples were analyzed and did not vary more than 10 percent.

The data from the Coulter Counter was used to calculate the nucleation and crystal growth rates. For example, a plot of  $\text{Log } N_L$  (cumulative number distribution) as a function of  $L$  (particle size) is shown in Figure 3.2 for Experiment G-30. From the intercept the nucleation rate is calculated to be  $1.5 \pm 0.2 \times 10^8 \text{ \#/m}^3\text{-sec}$ . The slope results in a linear growth rate of  $6.7 \pm 0.1 \times 10^{-9} \text{ m/sec}$ . This typical experiment produced solids that were rosette shaped. They varied in size from 10 to 160  $\mu\text{m}$ . The average particle size was approximately 40  $\mu\text{m}$ . The calcium sulfite hemihydrate content was  $85 \pm 3$  weight percent and the BET surface area was  $4.2 \pm 0.1 \text{ m}^2/\text{gram}$ .

The error in the nucleation rate depends on the errors in the slope and the total number of particles per liter ( $N_T$ ). The slope of the line depends on the particle size distribution and is not sensitive to small changes in each channel. Small changes are considered to be 10 percent of the channel value. This is the error in the Coulter Counter measurement. The slope error was within 2 percent for the majority of the experiments and within 5 percent for all experiments (see Appendix C for slope error analysis). The value of  $N_T$  has a  $\pm 10$  percent error. This results in an error in the intercept and therefore an error in the nucleation rate of  $\pm 10$  percent due to  $N_T$  alone. The total experimental error in the nucleation rate is between 10 and 15 percent for all experiments.

The effects of slurry solids concentration, solids residence time, pH, solution sulfate concentration, and temperature on the nucleation and growth rates were investigated. The product solids were characterized using scanning electron microscopy to determine crystal habit, iodine titration to determine sulfite content, and  $\text{N}_2$  absorption to determine BET surface area (for representative solids only).

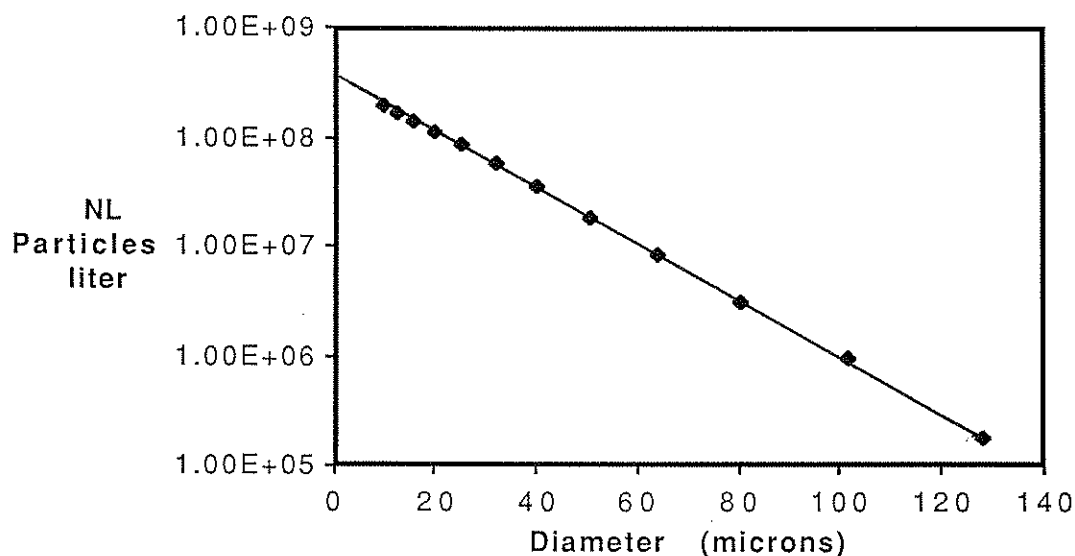


**Figure 3.2.** Typical Cumulative Number Distribution Plot

Experiment G-30 (pH=6.5, T=55°C,  $\tau$ =42 min.)

Feeds: 0.3M CaCl<sub>2</sub>, 0.08/0.02 M Na<sub>2</sub>SO<sub>3</sub>/Na<sub>2</sub>SO<sub>4</sub>

### 3.4 Results and Discussion

The nucleation and crystal growth rates of calcium sulfite hemihydrate were measured in a continuous flow crystallizer. The residence time of the solids was varied from 40 to 360 minutes. The solids density was varied from 7 to 90 grams per liter. The reactor pH was varied from 4.25 to 6.5. The majority of the experiments were performed at 55°C, but a few were performed at 25°C to determine the effect of temperature on the nucleation and growth rates. The gypsum saturation in the reactor was approximately 1.0 with a Ca<sup>++</sup> concentration of 100mM for these experiments. To determine the effect of gypsum saturation on the nucleation and growth rates, the gypsum saturation in the reactor was varied from zero to 0.7 with a Ca<sup>++</sup> concentration of 1mM. The pH was 6.5 to 6.75. A summary of the experimental data is contained in Table 3.1 and Table 3.2. This results in a power law equation that relates the



nucleation rate,  $B^0$  ( $\#/m^3\text{-sec}$ ) as a function is given by Equation (12) where  $M_T$  and  $G$  are the suspension density ( $kg/M^3$ ) and linear growth rate ( $m/sec$ ) respectively.

$$B^0 = 2.7 \times 10^{18} \exp\left(\frac{-4 \times 10^3}{RT}\right) M_T^{1.0} G^{1.0} \quad (12)$$

**Table 3.1** Summary of Experimental Data

Exp. #	S(IV) (end) (mM)	M <sub>T</sub> (end)		B <sup>0</sup> x 10 <sup>-8</sup>		G x 10 <sup>9</sup> (m/sec)	pH	τ (min)
		kg/m <sup>3</sup>		#/m <sup>3</sup> -sec)				
		Meas.	Pred.	Meas.	Pred.			
Base Case (55°C, Feed Streams: 0.3M CaCl <sub>2</sub> , 0.08M Na <sub>2</sub> SO <sub>3</sub> /0.02M Na <sub>2</sub> SO <sub>4</sub> )								
G-13	3.5	5.7	6.0	2.0	1.9	5.2	5.5	42
G-20	2.7	6.8	6.0	2.3	1.9	5.3	5.5	42
Effect of Suspension Density (2,4,4,12 times base feed concentrations for Na <sub>2</sub> SO <sub>3</sub> /Na <sub>2</sub> SO <sub>4</sub> and CaCl <sub>2</sub> )								
G-22	3.2	15.0	13.2	3.3	4.2	5.5	5.5	42
G-31	2.4	26.5	27.0	3.5	3.7	1.6	5.5	125
G-21	2.7	44.3	27.0	17	7.9	5.0	5.5	42
G-19	4.2	81.5	79.8	23	23	5.0	5.5	42
Effect of Residence Time								
G-24	2.1	6.3	6.1	1.1	0.68	1.9	5.5	125
G-25	2.3	6.7	6.1	0.25	0.16	0.46	5.5	360
Effect of Temperature (28°C)								
G-26	3.8	4.5	5.7	1.4	1.8	5.2	5.5	42
Three Feed System (55°C, 0.36M CaCl <sub>2</sub> ,0.096M NaHSO <sub>3</sub> /0.024M Na <sub>2</sub> SO <sub>4</sub> , 0.275M NaOH)								
G-15	1.7	8.9	6.3	1.5		9.0	6.0	42
G-16	0.8	7.8	6.2	1.1		9.0	6.5	42
Effect of Gypsum Saturation (55°C, 0.3M CaCl <sub>2</sub> , 0.1M Na <sub>2</sub> SO <sub>3</sub> /0 M Na <sub>2</sub> SO <sub>4</sub> )								
G-23	1.6	6.0	6.3	1.0		6.8	6.5	42
(55°C, 0.1M CaCl <sub>2</sub> , 0.3M Na <sub>2</sub> SO <sub>3</sub> /0 M Na <sub>2</sub> SO <sub>4</sub> )								
G-33	100	5.8	6.3	6.2		4.9	6.75	42
(55°C, 0.1M CaCl <sub>2</sub> , 0.12M Na <sub>2</sub> SO <sub>3</sub> /0.16M Na <sub>2</sub> SO <sub>4</sub> )								
G-36	12	6.9	6.3	1.4		9.0	6.75	42

**Table 3.1 (Continued) Summary of Experimental Data**

Exp. #	S(IV) (end)	M <sub>T</sub> (end)		B <sup>o</sup> x 10 <sup>-8</sup>		G x 10 <sup>9</sup>	pH	τ (min)
	(mM)	kg/m <sup>3</sup>		#/m <sup>3</sup> -sec		(m/sec)		
		Meas.	Pred.	Meas.	Pred			
Effect of pH								
G-35*	26.0	8.0	8.7	1.7		7.4	4.25	42
G-27	19.3	2.6	3.3	0.52		7.5	4.5	42
G-30	0.9	6.0	6.3	1.5		6.7	6.5	42
G-28	1.3	8.0	6.2	1.4		7.0	6.5	42

\* Feed concentrations double base case for Na<sub>2</sub>SO<sub>3</sub>/Na<sub>2</sub>SO<sub>4</sub> and CaCl<sub>2</sub>

### 3.4.1 Effect of Residence Time

The nucleation and crystal growth rates were determined at three different residence times: 40, 125, and 360 minutes. The suspension density was constant. The power law expression (Equation 11) can be used to determine the kinetic order  $j$  which relates the nucleation rate to the crystal growth rate. It was observed that the particle size distribution is independent of the residence time.

Figure 3.3 is a plot of  $\log B^0$  (nucleation rate) as a function of  $\log G$  (growth rate). The slope of this line is  $j = 0.9 \pm 0.1$ . Alvarez (1986) reported a value for the growth rate order of 1.1. Kelly (1983) also reported values of 0.94 and 1.1. His results also indicated that  $j$  does not vary significantly as a result of impurity addition to the solution. These results were obtained using significantly smaller residence times (10 to 30 minutes), smaller suspension densities (1 kg/m<sup>3</sup>), and a significantly different experimental apparatus. The fact that  $j=1$  implies that the growth rate and the nucleation rate have the same dependence on solution saturation.

Benson et al. (1988) used a power law model with a factor included to account for the power transferred to the slurry by the agitator. The experimental apparatus was much different than the one used in this study and others. It consisted of an 11.4 liter crystallizer with draft tubes and baffles. SO<sub>2</sub> was directly bubbled into the reactor or sulfurous acid was one feed stream. The second feed stream was a lime/magnesium hydroxide mixture. There was also a high speed centrifugal pump that circulated the

calcium sulfite solids between the crystallizer and an external vessel. They reported a value for the growth rate order of 0.63. The shear stresses imposed on the particles by the circulating pump caused the average particle size to decrease when the residence time increased. In general, previous researchers have presented little theory to explain observed growth rate orders. In the absence of known inhibitors, observed growth rate orders are in the range of 0.6 to 2.0.

Since the presence of additives, residence time, suspension density and reactor configuration (with low shear stress imposed on particles) do not affect the value of  $j$  significantly,  $j$  is set equal to 1.0. A kinetic order of 1.0 means that the growth rates change in proportion with the ratio of the residence times (Equation 13). Also, the particle size distributions of the solids for different residence times are the same. This is because the slope of the line in the cumulative population plot (see Figure 3.2) is obtained by the particle size distribution. The slope is  $1/G\tau$  and since  $G\tau$  is constant, the particle size distributions are the same. Therefore, larger particles cannot be obtained at longer residence times.

$$G_1\tau_1 = G_2\tau_2 \quad (13)$$

However, the size of calcium sulfite particles have been found by other investigators to be sensitive to the shear stress imposed on them by agitation and circulation pumps. This causes smaller particles to be generated at longer holding times. Different crystallizer configurations may have different growth rate orders.

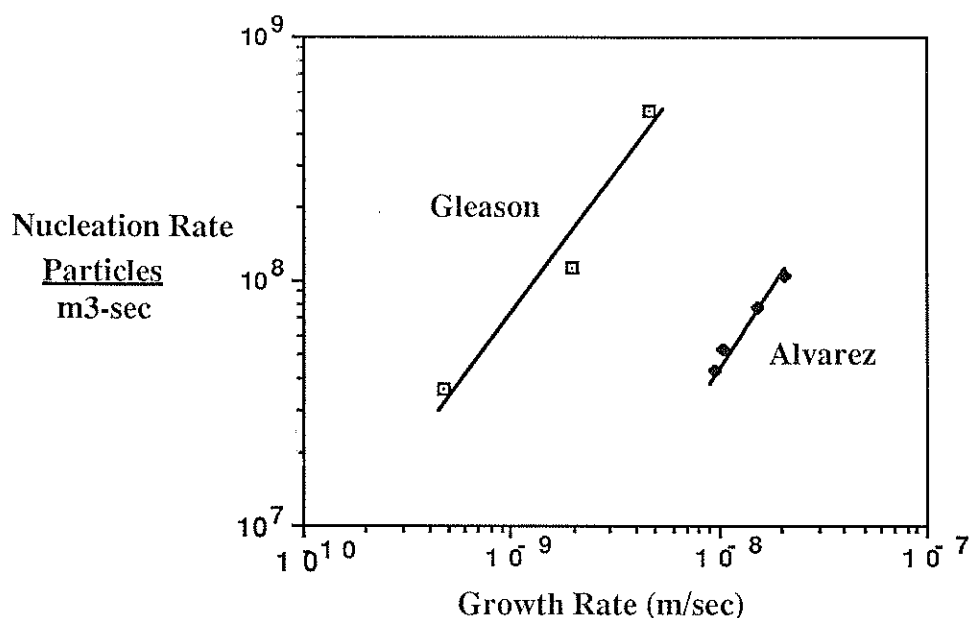


**Figure 3.3** Plot to Determine the Growth Rate Order.  
Effect of Residence Time

### 3.4.2 Effect of Suspension Density

The nucleation and crystal growth rates were determined at four suspension densities from 7 kg/m<sup>3</sup> to 90 kg/m<sup>3</sup>. The residence time was held constant at 42 minutes. The power law expression (Equation 11) was used to determine the kinetic order  $i$ , which relates the secondary nucleation rate to the solids in suspension ( $M_T^i$ ).

Figure 3.4 is a plot of  $\log B^0$  (nucleation rate) as a function of  $\log M_T$  (suspension density). The slope of this line is  $1.0 \pm 0.2$ . Therefore, the secondary nucleation is proportional to the suspension density. Table 3.1 contains the experimental data for the different suspension densities and shows that the growth rate is the same to within 10 percent except for Experiment G-31. Experiment G-31 was performed at a higher residence time ( $\tau=125$  min.). Since the growth rate order is equal

to 1.0, the product of the residence time and growth rate should be a constant (Equation 13).  $G\tau$  for the short residence time experiments (42 min.) was  $2.0 \times 10^{-7}$ . Experiment G-31 had a  $G\tau$  equal to  $2.1 \times 10^{-7}$ . Therefore, changing the suspension density of a system with linear secondary nucleation kinetics does not result in a size distribution change and the nucleation rate increases proportionally with the suspension density.

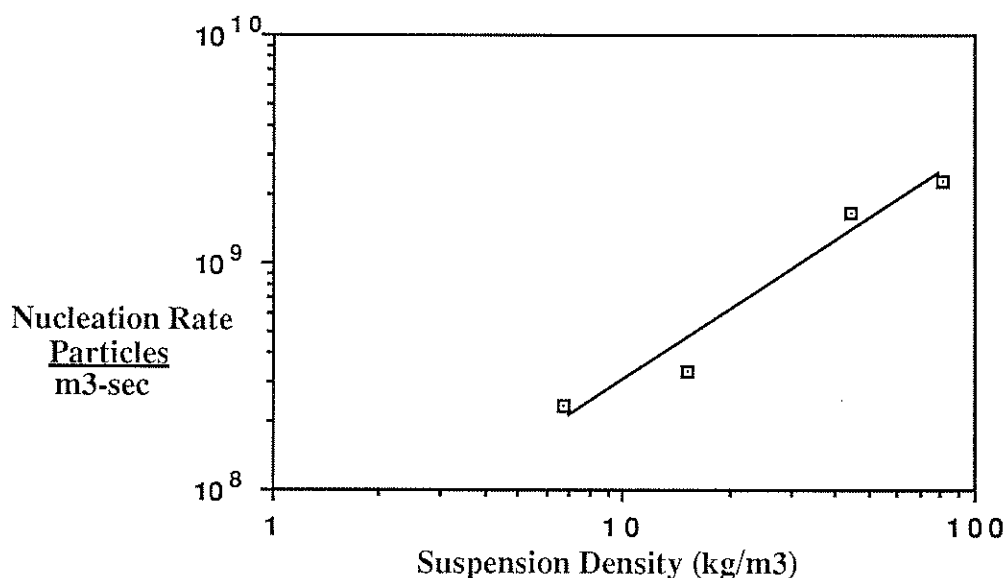


**Figure 3.4** Plot to Determine the Effect of Suspension Density on the Nucleation Rate

Other researchers studying calcium sulfite nucleation found that  $i$  is sensitive to other ions present in solution and the configuration of the experimental apparatus. Kelly (1983) found that  $i = 1.1$ . Alvarez-Dalama (1986) determined that  $i$  varied between 0.6 and 2.2 depending on whether  $\text{Cl}^-$  or  $\text{SO}_4^{2-}$  was present. Benson (1988) with different feed streams, the presence of magnesium, and much larger scale experimental apparatus (with a circulating pump) determined that  $i = 2.6$ . This higher order means that smaller particles were obtained at higher suspension densities probably due to the high shear stress imposed on the particles.

Because  $i$  is greater than zero, this is a process of secondary nucleation. Nuclei are created by the interaction of solids with shear caused by pumps and agitation. This mechanism should give  $i = 1$ . It does not appear that nuclei are produced by solid/solid interactions. If solid/solid interactions were important,  $i$  would be greater than 1.

The suspension density was measured by collecting and weighing the solids at the end of each experiment. It was also calculated using the difference between the sulfite concentrations in the feed stream and the reactor. Table 3.1 also contains these results. In most experiments the measured  $M_T$  is approximately 10 percent higher than the predicted. Scale formation on the reactor sides would cause the measured values of  $M_T$  to be higher than the predicted values. Two experiments produced less solids than predicted. These experiments were performed at low temperature and low pH. The total sulfite in solution for these experiments was greater than the base case. This is expected since at low pH and low temperature the sulfite-bisulfite equilibrium favors bisulfite. There are fewer sulfite ions in solution and therefore less solids precipitated.

Experiment G-21 had a much higher suspension density ( $44 \text{ kg/m}^3$ ) than the predicted value ( $27 \text{ kg/m}^3$ ). In this experiment the  $\text{CaCl}_2$  feed line split towards the end of the experiment. The  $\text{Na}_2\text{SO}_3$  feed stream was still operating. Since the  $\text{Ca}^{++}$  ion is in excess, more solids precipitated than expected.

In some of the preliminary experiments higher suspension densities also occurred. This was due to a failure in the level control. The solids were not withdrawn at a fast enough velocity. This caused a classified removal of the particles. More of the small particles were removed from the reactor than large particles. The resulting cumulative population plots were not straight lines (Figure 3.5).

Seven experiments failed due to improper level control. Four experiments failed due to the feed lines failing. These data have not been included in this analysis but are included in Appendix B. Seven additional experiments were not included in the analysis due to miscellaneous problems such as running out of sparge gas, incorrect solution compositions, and pH electrode drift.

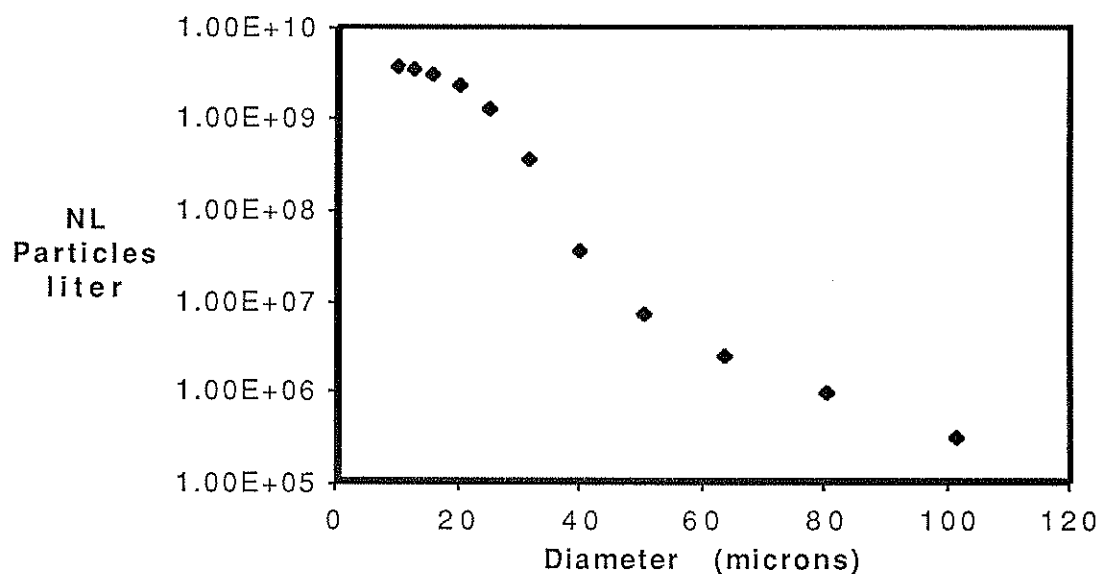


**Figure 3.5.** Cumulative Number Distribution Plot that Indicates Level Control Problems

Experiment G-18 (pH=5.5, T=55°C,  $\tau$ =42 min.)

Feeds: 1.2M CaCl<sub>2</sub>, 0.96M Na<sub>2</sub>SO<sub>3</sub>/0.24 Na<sub>2</sub>SO<sub>4</sub>

### 3.4.3 Effect of Temperature and pH

Experiments were performed at 28 °C to determine the effect of temperature on the nucleation and growth rates. Table 3.1 shows that the growth rate is constant over this range, but the nucleation rate increases as the temperature increases. The activation energy for CaSO<sub>3</sub> $\frac{1}{2}$ H<sub>2</sub>O nucleation is estimated to be 4±1 kcal/mole (Equation 14).

$$B^0 = K_n \exp\left(\frac{-4 \times 10^3}{RT}\right) M_T^{1.0} G^{1.0} \quad (14)$$

The significance of the activation energy is not apparent in this complex system. This is the activation energy for the nucleation rate as a function the growth rate. Tseng (1983) found that the activation energy was 10 kcal/mole when he related the growth rate as a function of calcium sulfite supersaturation to the second power. If we

substitute his value of the activation energy into Equation 14 we get an activation energy of 14 kcal/mole when the nucleation rate is a function of calcium sulfite supersaturation. This is consistent with surface kinetics mechanisms, but changes in the rate expression will change the activation energy.

The nucleation and growth rates were determined for pH values of 4.25, 4.5, 5.5, and 6.5. The nucleation rate constant was calculated from Equation 14 for all pH values. Figure 3.6 shows the nucleation rate constant ( $K_n$ ) as a function of pH. Although it appears that  $K_n$  has a maximum value near pH 5.5, an error analysis shows that the error in  $K_n$  is  $\pm 35$  percent for any single value of  $K_n$  (Appendix C). This indicates that at low pH the value of  $K_n$  is significantly lower than at pH 5.5, but there is no significant difference in the nucleation rate constant between pH values of 5.5 and 6.5.

This may be a tentative effect of pH, but in fact this might be an effect of gypsum saturation (sulfate in solution). Since less solids precipitated at the low pH values, there was more sulfate in solution (higher gypsum saturation). Gypsum saturation decreases the nucleation rate constant (see Section 3.4.4).



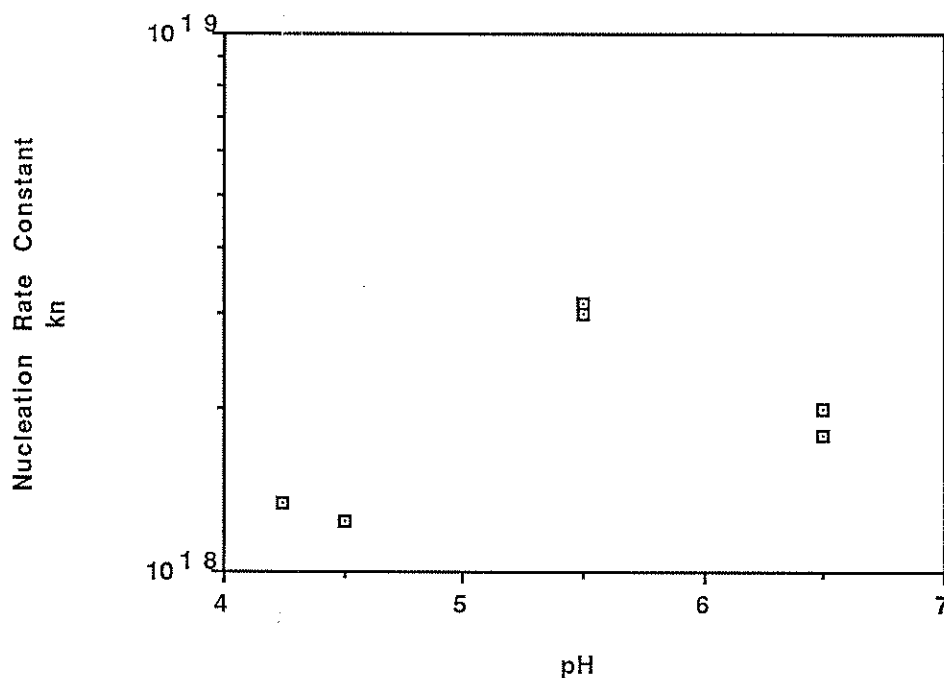


**Figure 3.6** Effect of pH on the Nucleation Constant

#### 3.4.4 Effect of Gypsum Saturation

The effect of dissolved sulfate (gypsum saturation) on the nucleation and growth rates was determined by a series of experiments in which the sulfite to calcium ion ratio ( $S(VI)/Ca^{++}$ ) in the feed streams was varied from zero to 1.6. This corresponds to a gypsum saturation change of zero to 1.0. Experiment G-28 had an excess of calcium ion while G-33 and G-36 were high in sulfite. The reactor pH was 6.5 to 6.75. Table 3.2 summarizes these results (see Table 3.1 for the complete experimental conditions). The nucleation rate constant ( $K_N$ ) was calculated from

Equation 14. Gypsum saturations were calculated using the Bechtel-Modified-Radian-Equilibrium Program (Lowell et al., 1970).

The weight percent  $\text{CaSO}_3 \frac{1}{2} \text{H}_2\text{O}$  of the product solids was determined by iodimetric titration. Table 3.2 shows that when there is no sulfate added to the feed streams the solids are 98 weight percent  $\text{CaSO}_3 \frac{1}{2} \text{H}_2\text{O}$ . As the gypsum saturation increases the weight percent  $\text{CaSO}_3 \frac{1}{2} \text{H}_2\text{O}$  decreases. The S(VI) to  $\text{Ca}^{++}$  ratio in the feed does not have a significant effect on the sulfite content of the solids. It appears that any sulfate in solution will end up in the solids up to approximately 80 weight percent. Then if the gypsum saturation is greater than 1.0 gypsum will also be precipitated.

Comparison of Experiments G-36 and G-28 indicate that nucleation and growth kinetics are not a function of calcium concentration in solution. When there is no sulfate added to the solution the nucleation rate constant ( $K_n$ ) increases by an order of magnitude over the experiments where sulfate is added. Clearly, the presence of sulfate in solution inhibits nucleation when expressed as a function of the growth rate. This was expected since in the batch experiments of Chapter 2, the presence of sulfate was found to inhibit both the dissolution and crystal growth rates of calcium sulfite hemihydrate. However, the nucleation rate is a stronger function of gypsum saturation than the growth rate when both are expressed as functions of calcium sulfite and gypsum supersaturation.

Since the nucleation rate is inhibited by the presence of sulfate (more so than the growth rate), larger particles should be formed in the presence of sulfate. Therefore, the use of oxidation inhibitors such as thiosulfate should actually reduce particle size because the gypsum saturation is very low. However, the dewatering properties of the low sulfate solids produced in the presence of thiosulfate are improved. Although the mean particle size is smaller or about the same, the particle shape is different. The low sulfate solids are thicker than the high sulfate solids (see Figures 2.1 and 2.2). These are the two seed crystals used in the batch experiments in Chapter 2. They have about

the same particle size distribution but were generated under potentially different nucleation conditions.

**Table 3.2** Effect of Gypsum Saturation

Exp.	$\frac{S(IV)}{Ca^{++}}$ M/M	$\frac{S(VI)}{Ca^{++}}$ M/M	$K_n \times 10^{-19}$ (#/kg-m)	RS Gypsum	$Ca^{++}$ mM	S(IV) mM	$CaSO_3 \cdot \frac{1}{2}H_2O$ wt %
G-33	3.0	0	12	0	0.6	100	98
G-36	1.2	1.6	1.0	0.22	0.8	12	86
G-28	0.27	0.07	1.2	1.0	100	1.3	81

### 3.4.5 Growth Rate Correlation

The growth rate is typically predicted by a power-law type expression (Equation 4) that relates the growth rate to the liquid supersaturation as in Chapter 2.

$$G = ks^a \quad (4)$$

Unfortunately, iodimetric titration to determine the total sulfite in solution was not accurate enough to distinguish small changes in supersaturation. This occurs when the total sulfite is in the 1-10 mM range. For example, if the precipitation rate is 0.1 M in 42 minutes (as in experiment G-20) and it takes 30 seconds to take a sample, 1-2 mM of sulfite could easily be lost as the solution approaches saturation. BMREQ was used to calculate the supersaturations of the reactor solutions using the measured total sulfite. In all cases, the supersaturations were very close to zero. Other researchers also observed this (Alvarez-Dalama, 1986, and Kelly, 1983).

### 3.4.6 Three Feed System

The experimental apparatus shown in Figure 3.1 has two feed streams,  $CaCl_2$  and a  $Na_2SO_3/Na_2SO_4$  mixture. The feed streams were fed below the liquid level. The crystals formed in all of these experiments were rosette-shaped. Figure 3.7 is an

example of the rosettes formed in the two feed system. There was some concern that there was inadequate mixing at the end of the feed tubes. This would result in areas of very high sulfite saturations. The Bechtel-Modified-Radian-Equilibrium Program (Lowell et al., 1970) was used to calculate the calcium sulfite relative saturations ( $RS_{CaSO_3}$ ) at the end of the feed tubes assuming an equal volume of feed and reactor solution for the base case experiment (G-20). At the end of the  $Na_2SO_3/Na_2SO_4$  feed tube the  $RS_{CaSO_3}$  is 15. The  $CaCl_2$  feed tube end has a  $RS_{CaSO_3}$  equal to 1.2. The bulk solution sulfite saturation is 1.0. In these areas there could be extremely fast nucleation resulting in rosette-shaped crystals.

Several experiments were performed with three feed streams to the reactor instead of two. The three feed streams were  $CaCl_2$ ,  $NaOH$ , and  $NaHSO_3/Na_2SO_4$  mix at flow rates that gave the same total reactor composition the same as the two feed system. The three feed system was investigated because at the ends of the three feed tubes there were not areas of high sulfite saturation. The  $RS_{CaSO_3}$  at the end of the  $NaHSO_3/Na_2SO_4$  feed tube was calculated to be 0.6. The  $CaCl_2$  and  $NaOH$  feed tube ends had sulfite saturations of 2.5 and 0.5 respectively. Hopefully platelets would be formed. This was not the case. The crystals formed were rosette-shaped (Figure 3.8) just as in the two feed system. In addition, pH control of the three feed system was difficult. The pH varied as much as 0.5 units above and below the desired pH. The nucleation rate constant ( $K_n$ ) was calculated to be  $1.1 \times 10^{18}$  compared to  $2.7 \times 10^{18}$  for the two feed system. Considering the difficulty in pH control of the three feed system this was acceptable. Therefore, the two feed system was used for all other experiments.

There were no mixing problems detected in the batch crystallization experiments in Chapter 2. In these experiments 0.02 to 0.2 M  $Na_2SO_3$  was titrated into 0.1M  $CaCl_2$  using the pH stat apparatus. These concentrations are comparable to those in the two feed nucleation experiments. The crystal habit of the batch solids did not change from platelet to agglomerates. A crystal habit change would indicate nucleation in the mixing zone. Furthermore, the particle size distribution did not change in a direction that would suggest that nucleation is occurring as a result of poor mixing.

Figure 3.7 SEM Photograph of Solids from Two Feed System  
Magnification 200X

Figure 3.8 SEM Photograph of Solids from Three Feed System  
Magnification 200X

### 3.5 Nomenclature

a	activity (mole/liter)
B	crystal birth function ( $\#/m^3\text{-m-sec}$ )
$B^0$	crystal nucleation rate ( $\#/m^3\text{-sec}$ )
D	crystal death function ( $\#/m^3\text{-m-sec}$ )
G	linear crystal growth rate (m/sec)
k	growth rate constant
$k_n$	nucleation rate constant
$K_{SP}$	calcium sulfite solubility product (mole/liter) <sup>2</sup>
L	crystal size (m)
$M_T$	total mass of particles ( $kg/m^3$ )
n	population density distribution function ( $\#/m^3\text{-m}$ )
$n^0$	nuclei population density ( $\#/m^3\text{-m}$ )
N	cumulative number distribution ( $\#/m^3$ )
$N_L$	number of particles greater than size L ( $\#/m^3$ )
Q	volumetric flow rate ( $m^3/sec$ )
RS	relative saturation of calcium sulfite hemihydrate ( $a_{Ca^{++}}a_{SO_3}/K_{sp}$ )
s	supersaturation as $1-RS$
t	time (sec)
V	total solution volume ( $m^3$ )

#### Greek Symbols

$\tau$	residence time ( $V/Q$ - sec)
--------	-------------------------------

## Chapter 4

### Conclusions and Recommendations

#### 4.1 Dissolution and Crystallization

Platelet shaped solids are generally formed in limestone slurry scrubbing processes. Agglomerates are formed in lime systems. Solids that have a high sulfate content are thinner and have slower settling rates. Platelets have better dewatering properties than agglomerates. Therefore it is important to determine the differences in the dissolution and crystallization rates for platelets and agglomerates. It is also important to determine if the solid sulfate content of the solids has an effect on the rates.

It was determined that there are subtle differences between platelet samples with different solid sulfate contents. There are also differences between platelet and agglomerated calcium sulfite. The platelet sample with a low solid sulfate content dissolved and crystallized slower than the platelet sample with a high solid sulfate content. Low sulfate platelets also dissolved and crystallized slower than the agglomerated samples. The inhibiting effect of dissolved sulfate was also greater for the sample with low solid sulfate. The sample with high solid sulfate dissolved and crystallized at approximately the same rate as the agglomerates.

#### 4.2 Nucleation and Crystal Growth

Nucleation and crystal growth rates can be used to predict particle size in crystallizers. These rates can also be used to examine prospects for increasing the

calcium sulfite particle size. This would result in faster settling rates and better dewatering properties. The nucleation and crystal growth rates of calcium sulfite hemihydrate were measured in a continuous flow crystallizer. Agglomerates were formed in the continuous flow crystallizer. The effects of solution sulfate concentration, residence time, suspension density and temperature on the rates were investigated.

It was determined that calcium sulfite exhibits typical linear secondary nucleation behavior which can be predicted by a power-law expression. The power law expression relates the nucleation rate to the suspension density, growth rate, temperature and other factors such as agitation. It was found that the nucleation rate was directly proportional to the suspension density and proportional to the growth rate. The particle size distribution does not change when the suspension density is changed. Also, when the nucleation rate is proportional to the growth rate, the product of the growth rate and the residence time is constant. Therefore the particle size distribution does not increase if the residence time is increased.

The activation energy for  $\text{CaSO}_3 \cdot \frac{1}{2}\text{H}_2\text{O}$  nucleation was estimated to be  $4 \pm 1$  kcal/mole. The nucleation rate constant was found to increase over the pH range of 4.5 to 5.5. Gypsum saturation in solution caused both the nucleation and growth rates to decrease.

#### 4.3 Industrial Applications

The purpose of nucleation and crystal growth studies of calcium sulfite hemihydrate are to improve the dewatering properties of the solids. This can be achieved by increasing the particle size or by changing the crystal habit. Since the nucleation rate is proportional to the growth rate, increasing the residence time of the solids will not increase the particle size. Also, the nucleation rate is proportional to the suspension density. Increasing the suspension density will not change the particle size. Other methods such as fines dissolution or classified solids removal must be used to improve the particle size. Oxidation inhibitors can be used to reduce gypsum



saturation and therefore grow thicker crystals. Other inhibitors could be used to change the crystal habit (make platelets instead of agglomerates).

Gypsum saturation was found to inhibit the dissolution of calcium sulfite. In forced oxidation systems, the calcium sulfite slurry is oxidized to calcium sulfate. Therefore it is probable that calcium sulfite dissolution is an important limiting mechanism in these processes.

#### **4.4 Recommendations for Future Work**

Calcium sulfite hemihydrate solids were formed as agglomerates in the continuous flow crystallizer. To measure the nucleation and growth rates of platelets, a different system must be used. A reactor that bubbles  $\text{SO}_2$  into a lime or limestone slurry with a separate continuous flow crystallizer could be used to generate platelets. This would be more like an industrial FGD system. The population balance approach could still be used to analyze the experiments.

Calcium sulfite has been found by others to be sensitive to the shear stress imposed on the particles by circulation pumps and agitation. A pump could be added in the experimental apparatus mentioned above to study the effects of high shear stress on the nucleation and growth rates. This circulating pump could also use to investigate the effects of fines dissolution on the particle size distribution and crystal habit. The effects of agitator speed could also be studied. Determining the conditions under which platelets are formed would be a major contribution to understanding FGD systems. Possibly high shear stress imposed on the particles and fines dissolution are reasons why platelets are formed.

It would be desirable to more closely simulate industrial solution compositions. This study suggests that the calcium sulfite supersaturation is very low. If this is true the interactions with sulfur dioxide removal and limestone dissolution are easily estimated by assuming saturated solutions. However, accurate solubility data is

necessary. This study determined that the solubility product of calcium sulfite is dependent on the sulfate content of the solids.

Additives and impurities are known to effect the nucleation and growth rates of many solids including calcium sulfite. More experiments could be performed with thiosulfate, or organic acids (additives in FGD systems) to determine their effects on the nucleation and growth rates. They have been shown to coprecipitate with calcium sulfite. Magnesium, iron, and manganese are known to inhibit limestone dissolution and are also impurities present in FGD systems. Their effect on calcium sulfite nucleation and crystal growth and also crystal habit could be investigated.

## Appendix A

### Analytical Methods

#### A.1 Iodimetric Titration

The clear solution samples collected during each experiment were analyzed for their sulfite concentration by iodimetric titration. Two ml of the sample was placed in 5 ml of pH 6 acetate buffer solution. The acetate buffer solution was composed of 1 M sodium acetate and 0.05 M acetic acid. A known amount of excess iodine was added to the solution and then titrated with standard sodium thiosulfate using starch as an endpoint indicator. For the blank test, the same procedures were repeated for 2 ml of distilled water instead of sample. The concentration of sulfite in the clear solution sample was determined from Equation A.1.

$$C = \frac{M(B-S)}{2V} \quad (A.1)$$

where:

- C = Concentration of sulfite (mole/liter)
- B = Volume of sodium thiosulfate used to titrate blank (ml)
- S = Volume of sodium thiosulfate used to titrate sample (ml)
- M = Concentration of sodium thiosulfate (mole/liter)
- V = Volume of sample (ml)

## A.2 Coulter Counter Methods

The slurry samples collected during each experiment were analyzed for the number of particles per ml and particle size distribution, with a Coulter Counter TAIL. The Sample Stand II was equipped with a 400 micron aperture which measures particles in the 8-200 micron range. the electrolyte used was 4 weight percent  $\text{CaCl}_2$  filtered to 0.5  $\mu\text{m}$ . Before each experiment the aperture was calibrated with 40.16  $\mu\text{m}$  standard particles.

One ml of the slurry was placed into a round bottomed sample beaker that contained 200 ml of electrolyte. For the experiments that had high solids concentration, only 0.4 ml of slurry was used. This was necessary to keep the solids concentration in the range for proper Coulter operation. The sampling switch was set in the MANOMETER position which measures the number of particles in a selected volume of electrolyte. Available volumes are 0.05, 0.5, and 2.0 ml. The 2.0 ml sample size was used for all runs.

The number of particles in the 2.0 ml volume was measured 3 to 5 times and averaged. Then the sampling switch was set to the TIME position and the particle size distribution (in differential volume percent) was measured. The collection time was 30 seconds. This was done 3 times and the results averaged. Number and size distribution data are in Appendix B. Dissolution or agglomeration the calcium sulfite particles was not observed over the measurement time.

The total number of particles in 500 ml of slurry ( $N_T$ ) was calculated from Equation A.2.

$$N_T = \frac{N(201 \text{ ml})(500 \text{ ml})}{(2 \text{ ml})(1 \text{ ml})} = N(5.025 \times 10^4) \quad (\text{A.2})$$

where:  $N$  = Number of particles collected in manometer mode.

The number of particles in each channel was calculated using  $N_T$  and the differential volume percentages. This method is based on the volumetric scaling in each channel. A particle in channel 3 has twice the volume in channel 2. The population in each channel ( $P_n$ ) is calculated from the differential volume percentages ( $V_n$ ) and the relative numbers ( $R_n$ ).

$$P_n = \frac{V_n R_n N_T}{(V_1 R_1 + V_2 R_2 + \dots V_{16} R_{16})} \quad (A.3)$$

**Table A.1** Channel and Relative Numbers

Channel No. (n)	Relative No. ( $R_n$ )
16	1
15	2
14	4
13	8
12	16
11	32
10	64
9	128
8	256
7	512
6	1024
5	2048
4	4096
3	8192
2	16384
1	32768

## Appendix B

### Experimental Data

#### B.1 Dissolution Experiments

Seed Crystals: Sample 1 (Acurex Sample)

Exp. No.	pH	Solution Composition			Dissolution Rate Constant $\times 10^{10}$ (cm <sup>2</sup> /sec)
		Ca <sup>++</sup> (mM)	S(IV) (mM)	S(VI) (mM)	
D-12	3.5	100	11	0	64.2
D-13	3.5	100	11	0	68.3
D-2	3.75	100	11	0	28.7
D-10	3.75	100	11	0	26.1
D-7	4.0	100	11	0	10.3
D-8	4.0	100	11	0	10.2
D-14	4.1	100	11	0	3.47
D-11	4.2	100	11	0	0.32
D-15	3.5	100	11	10	21.1
D-17	3.5	100	11	10	17.9
D-19	3.8	100	11	10	4.46
D-20	3.8	100	11	10	2.62
D-16	4.0	100	11	10	0.88
D-18	4.0	100	11	10	0.50

## Seed Crystals: Sample 2 (HLP Solids)

Exp. No.	pH	Solution Composition			Dissolution Rate Constant $\times 10^9$ (cm <sup>2</sup> /sec)
		Ca <sup>++</sup> (mM)	S(IV) (mM)	S(VI) (mM)	
I-26	3.5	100	11	0	27.2
I-28	3.5	100	11	0	21.8
I-22	3.7	100	11	0	14.9
I-25	3.7	100	11	0	15.6
I-23	3.9	100	11	0	7.98
I-27	3.9	100	11	0	7.27
I-3	4.0	100	11	0	5.36
I-7	4.0	100	11	0	5.74
I-17	4.0	100	11	0	5.95
I-9	4.1	100	11	0	4.19
I-13	4.1	100	11	0	4.25
I-10	4.2	100	11	0	2.44
I-14	4.2	100	11	0	2.55
I-11	4.3	100	11	0	1.46
I-15	4.3	100	11	0	1.68
I-19	4.3	100	11	0	1.42
I-12	4.4	100	11	0	0.27
I-18	4.4	100	11	0	0.26

## Seed Crystals: Sample 2 (HLP Solids)

Exp. No.	pH	Solution Composition			Dissolution Rate Constant $\times 10^9$ (cm <sup>2</sup> /sec)
		Ca <sup>++</sup> (mM)	S(IV) (mM)	S(VI) (mM)	
I-31	3.5	100	11	10	10.2
I-35	3.5	100	11	10	10.5
I-32	3.7	100	11	10	5.27
I-36	3.7	100	11	10	5.45
I-33	3.9	100	11	10	2.82
I-39	3.9	100	11	10	2.79
I-30	4.0	100	11	10	2.08
I-38	4.0	100	11	10	2.18
I-41	4.1	100	11	10	0.93
I-46	4.1	100	11	10	0.88
I-40	4.2	100	11	10	0.41
I-44	4.2	100	11	10	0.62
I-49	4.2	100	11	10	0.53
I-51	4.2	100	11	10	0.61
I-42	4.3	100	11	10	0.24
I-52	4.3	100	11	10	0.13
I-54	4.3	100	11	10	0.18
I-55	4.3	100	11	10	0.18

## B.2 Crystallization Experiments

Seed Crystals: Sample 1 (Acurex Low Sulfate Sample)

Solution Composition

Exp. No.	pH	Ca <sup>++</sup> (mM)	S(IV) (mM)	S(VI) (mM)	Relative Saturation		Growth Rate $\times 10^9 \left( \frac{\text{gmole}}{\text{min cm}^2} \right)$
					CaSO <sub>3</sub>	CaSO <sub>4</sub>	
C-1	4.7	100	10	0	2.0	0	1.05
C-2	5.0	100	10	0	3.5	0	5.10
C-3	5.25	100	10	0	5.2	0	30.6
C-4	5.5	100	10	0	7.3	0	223
C-5	6.0	100	10	0	11.3	0	895
C-6	5.25	100	10	5	5.1	0.5	8.60
C-7	5.25	100	10	10	5.0	1.0	9.55
C-8	5.25	100	10	20	4.8	2.0	1.18
Seed Crystals: Sample 2 (HLP High Sulfate Sample)							
N-5	4.8	100	10	0	1.8	0	0.70
N-2	5.0	100	10	0	2.8	0	12.8
N-1	5.25	100	10	0	4.3	0	40.1
N-3	5.5	100	10	0	5.9	0	207
N-4	6.0	100	10	0	9.1	0	414
C-6	5.25	100	10	5	4.1	0.5	31



### B.3 Nucleation and Crystal Growth Experiments

	G-3	G-4	G-5	G-6	G-7	G-8	G-9	G-10	G-11
DIAM(microns)	PERCENT	PERCENT	PERCENT	PERCENT	PERCENT	PERCENT	PERCENT	PERCENT	PERCENT
10.08	0.3	0.7	1.2	1.5	0.8	1.1	4.2	0.3	0.7
12.7	1	0.7	1.7	2.2	1	1.9	4.4	0.3	1.1
16	2.5	1.2	3.1	3.5	1.4	1.8	5.2	0.4	1.8
20.2	5.4	2.4	5.5	6	2.3	3.3	7.5	0.7	2.9
25.4	10.1	4.2	9.3	10.1	4.1	6	10.7	0.9	4.6
32	14.9	6.9	13.8	15.4	6.5	9.6	13	1.1	7.3
40.3	16.8	9.5	21.2	14.8	11.7	13.8	16	1.7	9.5
50.8	14.8	7.1	21.8	12.6	13.1	16.8	13.7	3	10.3
64	12	3.9	8.5	9	15.4	18.3	10.5	3.8	10.3
80.6	7.7	5.1	11.2	5.8	19.3	14.5	6.4	4.9	9.2
101.6	6.5	7.2	1.9	6.8	17.6	8.1	2.9	4.1	10.2
128	4.7	2.4	0.6	11.7	5	3.5	2.2	52.6	20.7
161	2.9	1.6	0.2	0.6	0.8	1.3	1.7	26.2	11.4
203	0	1.2			1	0	1.6	0	0
256						0	0		
Total Number	4.55E+11	2.74E+10	4.74E+12	2.83E+08	3.33E+08	2.88E+08	3.59E+08	2.30E+08	1.44E+08
Wt. %	82	84	83	84	79	40	80	97	81
CaSO <sub>3</sub> /2H <sub>2</sub> O									
BET Surface Area (m <sup>2</sup> /gram)					4.1				



G-22	G-23	G-24	G-25	G-26	G-27	G-28	G-29	G-30	G-31
PERCENT	PERCENT	PERCENT	PERCENT	PERCENT	PERCENT	PERCENT	PERCENT	PERCENT	PERCENT
0.5	2.2	1	1.9	0.7	0.6	0.3	0.4	0.4	0.5
0.9	2.9	1.8	3.7	1	0.7	0.4	1	0.7	1.2
2.1	3.9	3.1	7.6	1.8	1.3	0.7	3	1.4	3.2
6.2	5.4	4.8	13.9	3.1	2.6	1.3	7.2	2.9	7.4
12.6	7.2	7.2	17.9	5.7	4.1	2.6	12.5	5.6	11.8
17.7	10.7	12.6	18.3	12.7	7.2	5.3	19	10.4	14.1
12.9	11.2	16.9	14.1	19.9	10.9	8.8	20.4	14.3	16.6
14.6	13.8	21.3	10.5	26.1	14.3	14	18.9	16.5	17.9
12.5	14	15.6	7.7	16.9	19.5	18.1	11.2	17.8	14.2
12.2	12.2	9.5	3.3	7.5	17	18.9	5.3	14.6	10
6.1	7.4	6.2	1.1	3.8	12.5	16.7	1.1	10.4	2.6
1.7	5.2	0	0	0.8	7.4	7.9	0	5	0.5
0	3.9	0	0	0	1.9	3.2	0	0	0
0	0	0	0	0	0	1.8	0	0	0
1.83E+08	1.47E+08	7.31E+07	1.01E+08	8.66E+07	4.07E+07	6.02E+07	1.19E+09	9.89E+07	4.58E+08
75	88	83	16	82	79	81	24	85	82
	4.3								

G-32	G-33	G-34	G-35	G-36
PERCENT	PERCENT	PERCENT	PERCENT	PERCENT
0.2	2.9	0.8	0.3	2.3
0.4	3.8	1	0.5	1.8
1.1	5.1	0.8	0.6	1.8
2.8	7.6	1	1.4	1.8
6.1	10	1.5	2.8	2.3
11.2	13.1	2.4	5.5	3.3
15.6	15.6	5.7	10.2	5
21.1	16.9	10.3	16.5	7.6
19.5	13.6	15.8	19.3	12
16.3	6.5	22.2	19.1	14.5
5.2	4.9	23.3	14.4	16.9
0.5	0	12.8	7.3	18.5
0	0	2.4	1.7	10.3
0	0	0	0.4	1.9
1.21E+08	4.94E+08	9.83E+07	2.19E+08	3.39E+08
84	98	82	83	87

## Appendix C

### Error Analysis

#### C.1 Coulter Counter Measurements

The error in the number of particles in each channel depends on the total number of particles per volume and the volume percent in each channel. This will only address the error in the measured volume percent. The number of particles in each channel is given by Equation A.3 (see Appendix A).

$$P_n = \frac{V_n R_n N_T}{(V_1 R_1 + V_2 R_2 + \dots V_{16} R_{16})} \quad (A.3)$$

The derivative the number of particles in each channel (Equation A.3) with respect to the volume percent in each channel ( $R_n$  is a constant) is Equation C.1.

$$\frac{\partial P_n}{\partial V_n} = N_T \frac{(V_1 R_1 + V_2 R_2 + \dots V_{16} R_{16}) - V_n R_n^2}{(V_1 R_1 + \dots V_{16} R_{16})^2} \quad (C.1)$$

Equation C.1 was evaluated for each channel number to get the change in the number of particles in each channel.  $\Delta V_n$  is 10 percent of the volume percent in each channel ( $V_n$ ). This was done for each experiment using EXCEL. The change in slope of the cumulative population curves was evaluated using STATVIEW.

## C.2 Power Law Expression

The error in the nucleation rate constant can be estimated from the power law equation (Equation 14).

$$B^0 = K_n \exp\left(\frac{E_a}{RT}\right) M_T^i G^j \quad (14)$$

Take the natural log of Equation 14.

$$\ln B^0 = \ln K_n - \frac{E_a}{RT} + i \ln M_T + j \ln G \quad (C.2)$$

The derivative of Equation C.2 is Equation C.3.

$$d \ln B^0 = d(\ln K_n) - \frac{1}{RT} dE_a + i d(\ln M_T) + (\ln M_T) di + i d \ln G + (\ln G) dj \quad (C.3)$$

Equation C.3 is solved for  $d(\ln K_n)$  and calculated to be  $\pm 35$  percent using the errors in  $M_T$ ,  $G$ ,  $i$ ,  $j$ ,  $B^0$ , and  $E_a$  given in Chapter 3.

## List of References

- U.S. Environmental Protection Agency, Nationwide Emissions Report on National Air Quality Monitoring and Emissions Trends Report, EPA 450/2-78-052 (1978).
- Alvarez-Dalama, A., "Calcium Sulfit Hemihydrate Crystallization in Liquors with High Total Dissolved Solids", MS Thesis, University of Arizona (1986).
- Baczek, F., L.B. Benson, R.M. Golightley, and J. Wilhelm, "Effect of Wet Lime FGD Operating Conditions on Improving Particle Size and Dewatering of Sludge", EPA-600/9-87-004, 10-20, (1987).
- Benson, L.B., A. Randolph, and J. Wilhelm, "Improving Sludge Dewatering in Magnesium-Enhanced Lime FGD Systems", Presented at EPA/EPRI First Combined FGD and Dry SO<sub>2</sub> Control Symposium, St. Louis Mo., Oct. 1988.
- Bergland, K.A., E.L. Kaufman and M.A. Larson, "Growth of Contact Nuclei of Potassium Nitrate", *AIChE J.*, 25, 867 (1983).
- Bergland, K.A. and M.A. Larson, "Growth of Contact Nuclei of Citric Acid Monohydrate", *AIChE Symp. Ser.*, 78, 215, (1982).
- Bourne, J.R. and M. Zabelka, "The Influence of Gradual Classification on Continuous Crystallization", *Chem. Eng. Sci.*, 35, 533 (1980).
- Brown, C.A., G.M. Blythe, L.R. Humphries, R.F. Robards, R.A. Runyan, R.G. Rhudy, "Results from the RVA 10 MW Spray Dryer/ESP Evaluation", Presented at EPA/EPRI First Combined FGD and Dry SO<sub>2</sub> Control Symposium, St. Louis Mo., Oct. 1988.
- Burton, W. K., N. Cabrera, and F. C. Frank *Phil. Trans. Roy. Soc. (London)* A243, 299 (1951).
- Chan, P.K. and G.T. Rochelle, "Limestone Dissolution: Effects of pH, CO<sub>2</sub>, and Buffers Modeled by Mass Transfer," *ACS Symp. Ser.*, 188, 75-97, (1982).
- Chang, J.C., and N. Kaplan, "Pilot Evaluation of Limestone Regenerated Dual Alkali Processes", EPA/9-84-017, 5-21, (1984).
- Chang, J.C., J.H. Dempsey and N. Kaplan, "Pilot Testing of Limestone Regeneration in Dual Alkali Processes", EPRI-CS-2897, 201, (1983).
- Clontz, N.A., and W. B. McCabe, "Contact Nucleation of Magnesium Sulfate Heptahydrate", *Chem. Engr. Progr. Symp. Ser.*, 67, 110 (1971).

Cornell, C.G. and D.A. Dahlstrom, "Sulfur Dioxide Removal in a Double Alkali Plant", *Chem. Eng. Prog.*, 69 (12), 48 (1973).

Doyle, J.B. and B.J. Jankura, "Comparison of Dry Scrubbing Operation of Laramie River and Craig Stations," EPA-600/9-87-004, 9-22, (1987).

Edwards, L. O., "Calcium Sulfite Crystal Sizing Studies", EPA-600/7-79-192, (PB 80-128-689), August (1979).

Etherton, D., and A.D. Randolph, "Study of Gypsum Crystal Nucleation and Growth Rates in Simulated Flue Gas Desulfurization Liquors", EPRI Report CS-1885, June, 1981).

Garside, J., and S.F. Jancic, "Growth and Dissolution of Potash Alum Crystals in the Subsieve Size Range", *AIChE J.*, 22, 887 (1976).

Girolami, M.W., and R.W. Rousseau, "Size-Dependent Crystal Growth - A Manifestation of Growth Rate Dispersion in the Potassium Alum-Water System", *AIChE J.*, 31,1821 (1985).

Grootscholten, P.A.M., B.G.M. DeLeer, and E.J. DeJong, "Factors Affecting Secondary Nucleation Rate of Sodium Chloride in an Evaporative Crystallizer", *AIChE J.*, 28, 728 (1982).

Henzel, D.S., "Limestone FGD Scrubber Manual", EPA 68-02-3173, Feb, 1981.

Jarvis, J.B., F.B. Meserol, T.J. Selm, G.T. Rochelle, C.L. Gage, R.E. Moser, "Development of a Predictive Model for Limestone Dissolution in Wet FGD Systems", Presented at EPA/EPRI First Combined FGD and Dry SO<sub>2</sub> Control Symposium, St. Louis Mo., Oct. 1988.

Jones, B. J., P. S. Lowell, and F. B. Meserole, "Experimental and Theoretical Studies of Solid Solution Formation in Lime and Limestone SO<sub>2</sub> Scrubbers", EPA-600/2-76-273a (PB 264-953/AS ), Vol I October (1976).

Kelly, B. J., "Study of Calcium Sulfite Hemihydrate Nucleation and Growth Rates in Simulated Flue-Gas Desulfurization Liquors", MS Thesis, University of Arizona (1983).

Klimek, A.P., A.G. Eklund, G.W. Dawson, and D.M. Golden, "Design of Waste Management Systems for Calcium Spray Dryer FGD Technology", EPA-600/9-87-004, 10-76, (1987).

Liang, B.M., R.w. Hartel, and K.A.Bergland, "Growth Rate Dispersion in Seeded Batch Sucrose Crystallization", *AIChE J.*, 33, 2077 (1986).



Lowell, P.S., D.M. Ottmers, K. Schwitzgebel, T.I. Strange, and D.W. Deberry, "A Theoretical Description of the Limestone Injection Wet Scrubbing Process", EPA Report APTD 1287 (PB 193-029), Vol I, June(1970).

McCabe, W.L., "Crystal Growth in Aqueous solutions", *Ind. Eng. Chem.*, 21, 30, (1929)

Meserole, F.B. T.W Trofe, and D. A. Stewart, "Influence of High Dissolved Solids on Precipitation Kinetics and Solid Particle Size", EPA-600/9-84-017, 7-79, (1984).

Morasky, T.M., "Lime FGD Systems Data Book", EPA 68-02-2603, May 1979.

Ottmers, D., J. Philips, C. Burklin, W. Corbett, N. Phillips, and C. Shelton, "A Theoretical and Experimental Study of the Lime/Limestone Wet Scrubbing Process", EPA-650/2-75-006 (PB 243-399/AS), December (1974).

Peters, R.W., and J.D. Stevens, "Effect of Iron as a Trace Impurity on the Water Softening Process", *AIChE Symp. Ser.*, 78,46 (1982).

Philips, J.L., J.C. Terry, K.C. Wilde, G.P. Behrens, P.S. Lowell, J.L. Skloss and K.W. Luke, "Development of a Mathematical Basis for Relating Sludge Properties to FGD-Scrubber Operating Variables", EPA-600/7-78-072, April 1978.

Quian, R., Z. Chen, H. Ni, Z. Fan, F. Cai, "Crystallization Kinetics of Potassium Chloride from Brine and Scale-up Criterion", *AIChE J.*, 33, 1690 (1987).

Randolph, A.D., and M.D. Cise, "Nucleation Kinetics of the Potassium Sulfate-Water System", *AIChE J.*, 18,798 (1972).

Randolph, A. D., and M. A. Larson, Theory of Particulate Processes, Academic Press, New York (1971).

Randolph, A.D. and A.D. Puri, "Effect of Chemical Modifiers on Borax Crystal Growth, Nucleation and Habit", *AIChE J.*, 27, 92 (1981).

Rochelle, G.T., "Desulfurization, Gas, Stack Gas", *Encyclopedia of Chemical Technology*, J.J. McKetta (Editor), 15,145-163 (1982).

Reinauer, T.V., J.P. Monat, and M. Mutsakis, "Dry FGD on an Industrial Boiler", *Chem. Eng. Prog.*, 79(3), 74, (1983).

Rochelle, G.T, .P.T. Chan, and A.T. Toprac, "Limestone Dissolution in Flue Gas Desulfurization Processed", EPA Report No. PB 83-52833, April 1983.

Rochelle, G.T. and C.J. King, "Alternatives for Stack Gas Desulfurization by Throwaway Scrubbing", *Chem. Eng. Prog.*, 74(2), 65 (1978).

Setoyama, K. and S. Takahashi, "Solid Solution of Calcium Sulfite Hemihydrate and Calcium Sulfate", *Yogyo-Kyokai-Shi*, 86, 56-62 (1978).

Shor, S.M. and M.a. Larson, "Effect of Additives on Crystallization Kinetics", *Chem. Eng. Prog. Symp. Ser.*, 110, 32 (1971).

Sikdar, S.K., F. Ore, and J.H. Moore, "Crystallization of Calcium Sulfate Hemihydrate in Reagent-Grade Phosphoric Acid", *AIChE Symposium Series*, No.193, Vol 76, 1980.

Simpson, J.L. and J.H. Wilhelm, "Development and Demonstration of a Limestone Dual Alkali FGD Process at Central Illinois Public Service Company's Newton Power Station", EPA-600/9-85-033, 430, (1985).

Strickland-Constable, R.F., "The Breeding of Crystal Nuclei - A Review of the Subject", *AIChE Symposium Series*, No.121, Vol 68, 1980.

Tomlinson, G.H., "Air Pollutants and Forest Decline", *Environ. Sci. Technol.*, 17:246 (1983).

Toprac, A. J., "Limestone Dissolution in Stack Gas Desulfurization", *Env. Prog.*, 1, 52-58 (1982).

Tseng, P. C., "Calcium Sulfite Hemihydrate Dissolution and Crystallization", PhD Dissertation, University of Texas Austin (1983).

Tseng, P.C. and G.T. Rochelle, "Dissolution Rate of Calcium Sulfite Hemihydrate in Flue Gas Desulfurization Processes", *Env. Prog.*, 5, 35-40 (1986a).

Tseng, P.C. and G.T. Rochelle, "Calcium Sulfite Hemihydrate: Crystal Growth Rate and Crystal Habit", *Env. Prog.*, 5, 5-11 (1986b).

Van Rosmalen, G. M., Scale Prevention, Delft University Press, the Netherlands (1981).

Youngquist, G.R. and A.D. Randolph, "Secondary Nucleation in a Class II System: Ammonium Sulfate-Water", *AIChE J.*, 18, 421 (1972).

Zumstein, R.C., and R.W. Rousseau, "Growth Rate Dispersion by Initial Growth Rate Distributions and Growth Rate Fluctuations", *AIChE J.*, 33, 121 (1987).

## VITA

Cynthia Lynn Gleason was born in Madison, Wisconsin on July 11, 1954, the daughter of Keith and Kathleen Cooley. After graduation from Lafollette High School, Madison, Wisconsin in 1972, she entered the University of Wisconsin at Madison for one year. During the years 1973-1976 she lived in Illinois and Colorado with her husband William Gleason, who was in the United States Air Force. She returned to the University of Wisconsin at Madison in 1976 to continue her education and completed her BS in Chemical Engineering in May 1980. Then she worked for General Electric Corporate Research and Development in Schenectady, New York for 3 years. In January, 1983 she entered the graduate school of the University of Texas at Austin. After graduating with her Ph.D. in August of 1989, she will move to Nashua, New Hampshire.

Permanent Address:  
c/o Keith Cooley  
5306 Hoboken Rd.  
Madison, WI 53713

This dissertation was typed by the author.